LITHOLOGIC AND TECTONIC CONTROLS ON BEDROCK CHANNEL FORM AT THE NORTHWEST HIMALAYAN FRONT

George Henry Allen

A thesis submitted to the faculty of the University of North Carolina at Chapel Hill in partial fulfillment of the requirements for the degree of Master of Science in the Department of Geological Sciences.

Chapel Hill
2012

Approved by:

Dr. Jason B. Barnes

Dr. Tamlin M. Pavelsky

Dr. Eric Kirby

ABSTRACT

GEORGE HENRY ALLEN: Lithologic and Tectonic Controls on Bedrock Channel Form at the Northwest Himalayan Front
(Under the direction of Dr. Jason Barnes)

Recognition that channel form reflects a river's ability to erode rock has spawned stream-power models that estimate patterns of incision by approximating energy dissipation within a channel. Most commonly, these models assume channel width exponentially scales with drainage area, in part, because drainage area is easily extracted from digital elevation models (DEMs). However, this assumption is often confounded by local variations in rock strength and uplift rate that cause channel constriction downstream. Here we investigate the morphological response of 10 bedrock channels traversing the Mohand range at the northwest Himalayan front to spatial changes in rock strength and uplift rate. We present a new method to continuously measure and compare channel width, slope, and other hydraulic parameters using satellite image analysis and a DEM. Our results suggest that rock strength importantly influences channel form and that channel width should be explicitly measured when extracting tectonic signals from channel morphology.

ACKNOWLEDGEMENTS

I thank my advisor, Dr. Jason Barnes for his exceptional guidance and attention to detail throughout this research project. Dr. Tamlin Pavelsky and Dr. Eric Kirby were invaluable resources and provided useful comments to improve this manuscript. I also thank Dr. Vikrant Jain, Dr. Vimal Singh, Aravind Nair, Rakesh Malhotra, and K.K. Sharma for help with the fieldwork and logistics. Dr. Jonathon Lees and Dr. Brian Yanites provided analytical and technical advice, and Dr. Rajiv Sinha for providing Spot 5 imagery. Financial support was provided by NSF EAR 0814723 to J. Barnes and by the UNC Martin Fund and a GSA Graduate Research Grant to G. Allen. Finally, I give a special thanks to my family for encouraging me to pursue a graduate degree.

TABLE OF CONTENTS

LIST OF FIGURES

Figure

LIST OF SYMBOLS

A ..... Upstream drainage area

a_e ..... Incision efficiency exponent

b ..... Width exponent

b_{ref} ..... Reference wideness exponent

c ..... Runoff exponent

E ..... Incision rate

$f(q_s)$ ..... Entrained sediment function

g ..... Gravity

K' ..... Stream power coefficient

k_e ..... Incision efficiency coefficient

k_q ..... Runoff coefficient

k_s ..... Steepness index

k_{sn} ..... Normalized steepness index

k_t ..... Shear stress coefficient

k_w ..... Width coefficient

k_{wn} ..... Normalized wideness index

m' ..... Upstream drainage area exponent

n ..... Manning friction factor

n' ..... Width exponent

Q ..... Discharge

S ..... Channel slope

U ..... Rock uplift rate

W ..... Channel width

W_e ..... Equilibrium channel width

α ..... Width-discharge exponent

β ..... Channel slope exponent

θ ..... Concavity index

θ_{ref} ..... Reference concavity index

ρ ..... Water density

τ_b ..... Boundary shear stress

τ_c ..... Critical shear stress

τ_{ind} ..... Shear stress index

CHAPTER I

LITHOLOGIC AND TECTONIC CONTROLS ON BEDROCK CHANNEL FORM AT THE NORTHWEST HIMALAYAN FRONT

1. INTRODUCTION

In mountainous terrain, bedrock river channels encode signals of tectonic and climatic forcings [*Whittaker*, 2012]. Hillslope gradient and relief have also been proposed as metrics of erosion, however thresholds in hillslope transport processes lead to saturation at relatively low erosion rates [*Montgomery and Brandon*, 2002; *Ouimet et al.*, 2009]. Bedrock rivers themselves control the long-term denudation rates of mountain belts by setting base level for hillslope processes, incising into rock and transporting material from mountain belts [*Burbank et al.*, 1996; *Molnar and England*, 1990]. Further, they dictate the first order response of mountain ranges to external forcings by communicating tectonic and climatic signals across the landscape through adjustment of their channel form [see review *Kirby and Whipple*, 2012]. Given this connection between bedrock river form and forcing, it is now thought that tectonic and climatic information can be extracted from patterns of bedrock channel geometry [see review *Wobus et al.*, 2006a]. Unfortunately, establishing the link between a particular forcing and channel form is often challenging because the latter may also reflect adjustment to other factors including substrate erodibility, sediment supply, hydraulic roughness, vegetation, and hillslope processes that vary in space and time [*Duvall et al.*, 2004;

Finnegan et al., 2007; *Goode and Wohl*, 2010; *Montgomery et al.*, 1996; *Walsh et al.*, 2012; *Whittaker et al.*, 2008].

Channel form reflects river erosional capacity because rivers with steep and narrow channels flow faster over a smaller area, focusing more energy on the bed to erode rock and transport sediment. Shear stress stream-power models use channel form to estimate patterns of bedrock incision by approximating energy dissipation within a channel [*Finnegan et al.*, 2005; *Howard*, 1994; *Howard and Kerby*, 1983; *Whipple and Tucker*, 1999]. These models most commonly focus on changes in channel slope because slope controls the rate of potential energy expenditure per downstream distance and changes in width are more difficult to measure in rugged terrain [*Wobus et al.*, 2008]. However, lateral channel adjustments may be equally important because width represents another way that channels can respond to changing boundary conditions [*Stark*, 2006; *Turowski et al.*, 2008; *Wobus et al.*, 2006b; *Yanites et al.*, 2010].

Field-based studies have empirically determined channel width and used these measurements in the context of stream-power models [*Amos and Burbank*, 2007; *Anderson*, 1994; *Duvall et al.*, 2004; *Harbor*, 1998; *Lavé and Avouac*, 2000, 2001; *Snyder et al.*, 2003a; *Stock and Montgomery*, 1999; *Tomkin et al.*, 2003; *Whittaker et al.*, 2007b; *Yanites et al.*, 2010]. However, these studies were only able to make large-scale conclusions about bedrock channel process and adjustment because width was sampled at a coarse spatial resolution downstream (e.g. every 100 m in *Finnegan et al.*, [2005]). Coarse sampling of changes in channel width may inhibit our understanding of bedrock channel response to perturbations because width can change significantly over short length scales. Observations of channel gradient alone may bias interpretations because

rivers adjust their gradients and widths differently to variations in lithology [*Montgomery and Gran*, 2001] or rock uplift rate [*Yanites et al.*, 2010]. Continuous measurement of both vertical and lateral channel geometry may further our knowledge of channel adjustment tectonic and lithologic variations in an actively uplifting equilibrium setting (i.e. where the channel morphology is presumably adjusted to prevailing tectonic and climatic conditions). Further, given the fact that substrate erodibility is variable at many scales, important controls on channel morphology and incision patterns may currently be overlooked.

In steady-state landscapes (i.e. dynamic equilibrium between relative base level lowering and incision), rivers balance downstream increases in rock strength and uplift rate by adjusting their channel form to generate increased stream power for a given discharge [*Kirby and Whipple*, 2012]. An increase in stream power causes a larger proportion of flow to surpass a critical discharge necessary to move sediment [*Gilbert*, 1877; *Sklar and Dietrich*, 1998]. If sediment supply is high relative to transport capacity, material deposited on the channel bed inhibits vertical incision, promotes lateral erosion, and hence widens channels [*Finnegan et al.*, 2007]. Thus, given adequate sediment supply, changes in rock strength or uplift rate can alter the distribution of erosion within a channel and may lead to a decoupling between slope and width adjustments. We hypothesize that where rock strength or uplift rate varies downstream, channel width adjustments may vary independently from changes in drainage area and/or slope. We test these ideas by applying a new method that integrates satellite image and digital topographic analysis to estimate bedrock channel width and slope continuously downstream along channels traversing the uplifting Mohand range at the northwest

Himalayan front in India. The Mohand range is an ideal natural laboratory for exploring channel adjustment to changes in rock erodibility and uplift rate because these factors vary in systemic ways across the region.

2. DOWNSTREAM HYDRAULIC SCALING

In theory, channels evolve towards a form that expends the minimum amount of total energy and distribute this energy dissipation evenly throughout the fluvial network [*Langbein and Leopold*, 1964; *Stølum*, 1996]. If tectonic and climatic conditions do not vary over long periods of time (>100 kyrs in most settings), bedrock channel morphology converges towards an equilibrium form whereby incision and rock uplift rate are balanced [*Whipple*, 2004]. If other factors that affect channel morphology (e.g. substrate erodibility, sediment supply and grain size distribution) remain uniform, the equilibrium shape exhibits well-documented hydraulic scaling relationships similar to those observed in self-formed alluvial rivers [*Wohl*, 2004; *Wohl and David*, 2008]. Hydraulic scaling relates longitudinal and cross sectional channel geometry to discharge with theoretically and empirically derived exponential functions [*Hack*, 1957; *Leopold and Maddock*, 1953].

2.1 Channel Slope

Channel slope regulates the rate at which potential energy is lost per unit downstream distance and is often considered the most important hydraulic parameter for estimating incision [e.g. *Howard and Kerby*, 1983; *Lavé and Avouac*, 2001]. Equilibrium channels display a graded profile described by a power-law relationship between local slope (S) and contributing upstream drainage area (A),

$$S = k_s A^{-\theta}, \quad (1)$$

where k_s is the steepness index and θ is the concavity index (Figure 1a, b) [*Flint,* 1974]. The concavity index is determined by fitting a linear regression to slope-area data from the equilibrium channel reaches (i.e. those without knickpoints, rock uplift rate gradients, or changes in substrate downstream) (Figure 1c) [*Wobus et al.*, 2006a]. To compare steepness across channel segments with varying drainage areas and concavity indices, a regional mean concavity index is determined and used as a reference (θ_{ref}), allowing for the empirical calculation of the normalized steepness index,

$$k_{sn} = SA^{-\theta_{ref}}, \quad (2)$$

a measure of relative steepness (Figure 1d) [*Wobus et al.*, 2006a]. Normalized steepness is a useful metric because it can be automatically extracted from digital elevation models (DEMs) and has been shown to correlate with erosion rate [*Kirby and Whipple*, 2012].

2.2 Channel Width

Channel width determines the quantity of energy exerted on a channel's bed per unit area, with a reduction in width focusing this energy and enhancing incision. Equilibrium channels exhibit an exponential relationship between width (W) and upstream drainage area,

$$W = k_w A^b \tag{3}$$

where k_w is the width coefficient, and b is the width exponent ($b \cong 0.5$) (Figure 1e, f) [*Hack*, 1957; *Montgomery and Gran*, 2001; *Snyder et al.*, 2003a]. The width coefficient can be thought of and used as an empirical parameter of channel geometry, but it can also be directly related to incision potential based on stream-power models. By combining incision models under the assumptions of steady-state equilibrium and that slope scales exponentially with drainage area, the width coefficient, hereinafter referred to as the wideness index, can be considered the lateral component of channel adjustment related to incision potential (Appendix A). Similar to θ_{ref} in equation (2), a mean width exponent can be determined for equilibrium channel reaches, yielding a reference wideness exponent (b_{ref}) (Figure 1g). Applying b_{ref} to width-area data produces the normalized wideness index,

$$k_{wn} = W A^{b_{ref}}, \tag{4}$$

a parameter that allows for quantitative comparison of channel widths across a region (Figure 1h). We consider downstream variations in k_{wn} to be an empirical measure of the deviation from a regional equilibrium width-area scaling, set by b_{ref}.

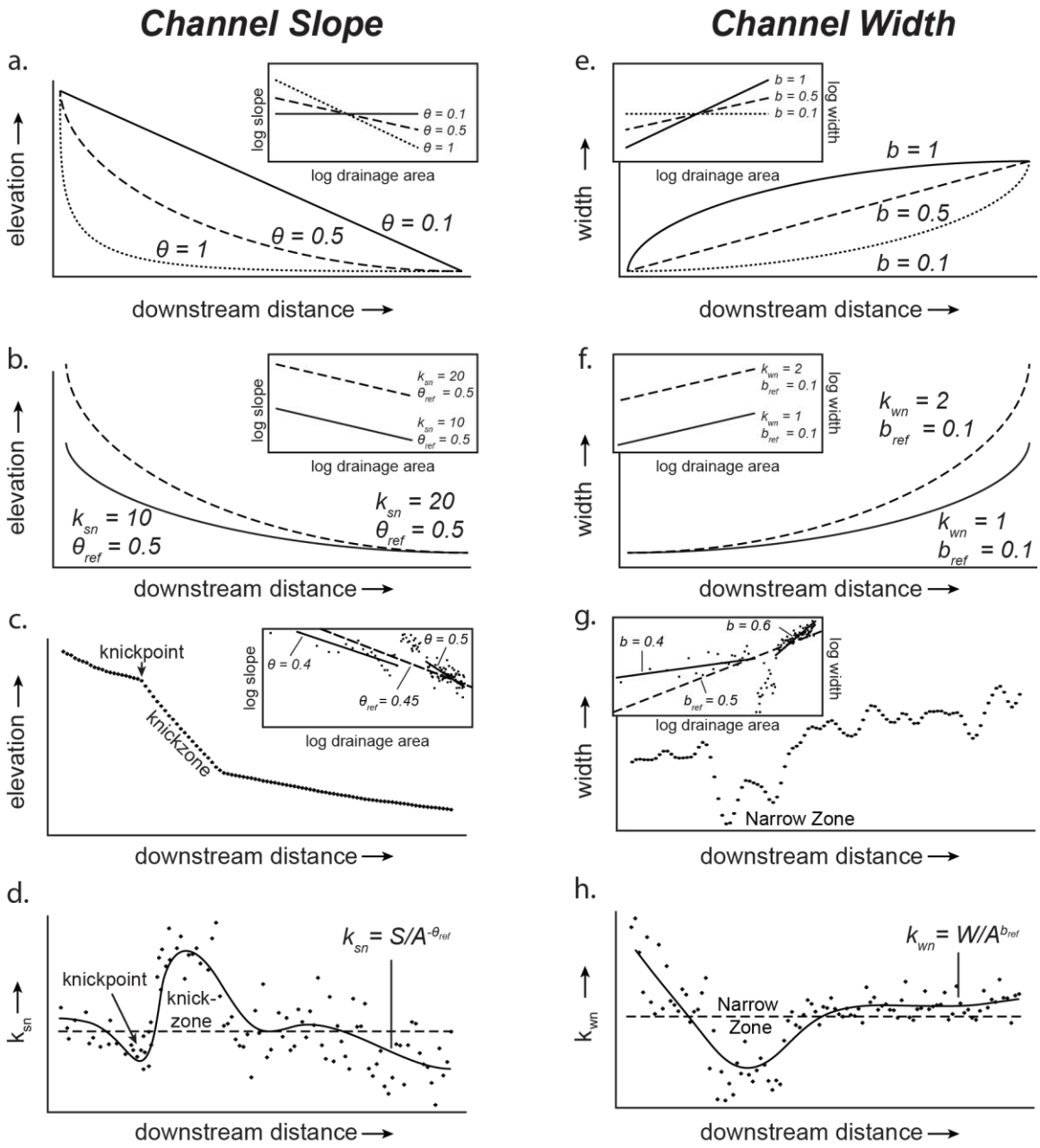

Figure 1. Idealized variations in channel form parameters downstream. Equilibrium long profiles with varying concavity indices (a) and steepness indices (b) with insets displaying slope-area data [modified after *Duvall et al.*, 2004; *Whipple and Tucker*, 1999]. (c) Long profile with a knickpoint and knickzone. Inset shows reference concavity (slope of dashed line) set by linear regressions through the equilibrium slope-area reaches (gray lines). (d) Long profile of raw (dots) and smoothed (line) normalized steepness index (k_{sn}) from profile in part c. Dashed horizontal line is mean k_{sn} and equivalent to θ_{ref} (inset of part c). (e) Equilibrium channel width long profiles with varying width exponents assuming a square increase in drainage area with increasing distance downstream. Inset is the width-area data. (f) Equilibrium long width profiles with varying wideness indices (k_{wn}) and fixed width exponent b. Inset shows same profiles in width-area space. (g) Idealized width long profile with an intermediate narrow zone. Inset shows reference width exponent (dashed line slope) determined by linear regressions through equilibrium width-area reaches (gray lines). (h) Long profile of raw (dots) and smoothed (line) normalized wideness index (k_{wn}). Dashed horizontal line is average k_{wn} and equivalent to b_{ref} (inset of part g).

3. GEOLOGIC AND GEOMORPHIC SETTING

Considerable convergence of India with Asia (~20 of ~40 mm/yr) has been focused near the Himalayan front in the Quaternary [*Bilham et al.*, 1997; *England and Molnar*, 1997; *Kumar et al.*, 2001]. Much of this convergence is accommodated along the Himalayan Frontal Thrust (HFT) [*Lavé and Avouac*, 2001; *Wesnousky et al.*, 1999]. The HFT is a segmented, blind-to-emergent fault recognized as the main tectonic and topographic boundary (or discontinuity) between the Himalayas and the Gangetic foreland (Figure 2) [*Kumar et al.*, 2006; *Nakata*, 1989]. Shortening along the HFT drives uplift of foothill ranges that are composed of Tertiary molasse deposits of the Siwalik Group that hence are called the Siwalik Hills [*Malik and Nakata*, 2003; *Yeats and Lillie*, 1991; *Yeats and Thakur*, 2008]. Bedrock rivers draining the Siwalik Hills are argued to be in steady-state equilibrium with the active faulting because (1) patterns in river incision potential match rock uplift rates inferred by dated fluvial terraces [*Lavé and Avouac*, 2000, 2001], (2) channels exhibit well-graded elevation profiles where rock types and uplift do not vary [*Kirby and Whipple*, 2001], and (3) a combination of weak uplifting rock and high river discharge during monsoons provide erosionally efficient river and overland flow that keeps hillslopes near failure by landsliding and allows channels to rapidly adjust to the active deformation [*Barnes et al.*, 2011].

In northwestern India, the Mohand range is a Siwalik uplift structure that is ~80 by 15 km long with ~500 m of total relief (Figure 2) [*Rao et al.*, 1975]. Geologic and geophysical data indicate the Mohand is a fault-bend fold in the HFT hanging wall [*Kumar et al.*, 2006; *Powers et al.*, 1998; *Wesnousky et al.*, 1999]. Here, the HFT has slipped ~4-5 km along a variably-dipping (~30-20°NE) ramp that changes into a flat

close to the southwestern mountain front near the fold axis (Figure 2b) [*Mishra and Mukhopadhyay*, 2002; *Powers et al.*, 1998]. As a consequence of this fault geometry, average rock uplift rates between the range flanks vary [*Barnes et al.*, 2011], but are approximately uniform and high across most of the southern flank [*Kirby and Whipple*, 2012]. However, near the range front, the HFT ramp dip goes to zero resulting in a zone of little to no rock uplift. Regional magnetostratigraphy data from the Siwaliks rocks suggest Mohand deformation began <~0.8 Ma [*Sangode and Kumar*, 2003]. Near the town of Mohand, a radiocarbon dated uplifted fluvial terrace suggests a HFT slip rate of ≥13.8 ± 3.16 mm/a and a rock uplift rate of 6.9 ± 1.8 mm/a [*Wesnousky et al.*, 1999].

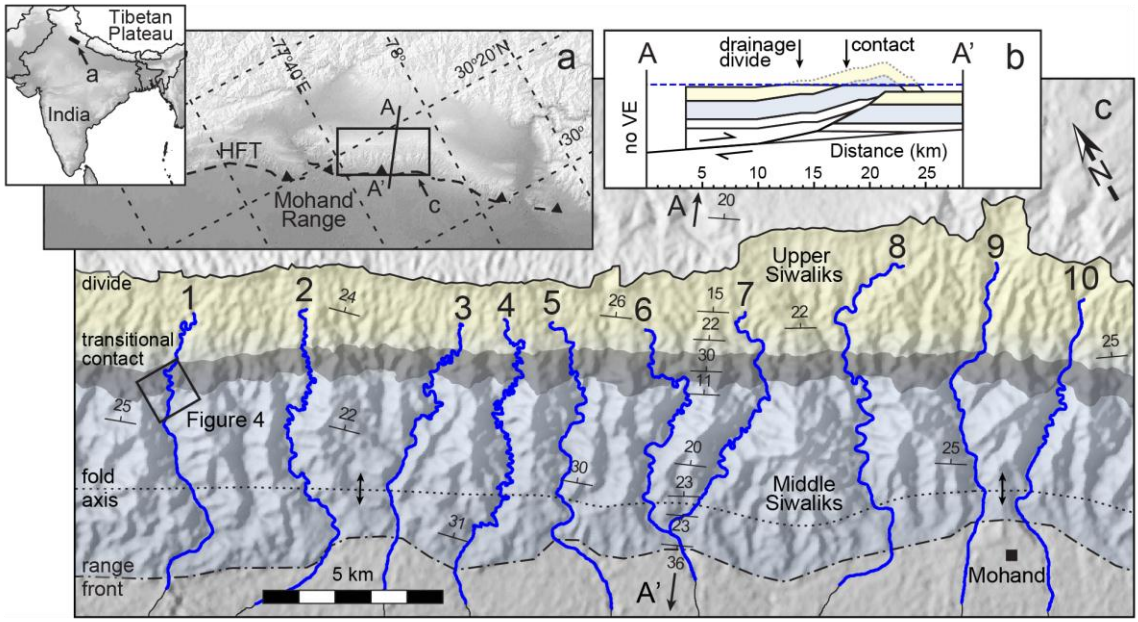

Figure 2. The Mohand range in the Siwalik Hills, northwest India. (a) The topography results from hanging wall uplift above a Himalayan Frontal Thrust (HFT) segment [fault from *Raiverman et al.*, 1990]. (b) Balanced cross section through the central Mohand [simplified from *Barnes et al.*, 2011; *Mishra and Mukhopadhyay*, 2002]. Blue dashed line is the mean channel elevation. (c) The 10 study area channels flowing southward from the central portion of the range. Channels begin in Upper Siwaliks conglomerates (yellow), cross a transitional contact (dark grey), then traverse Middle Siwaliks sandstones (blue-gray) before entering the foreland. South of the fold axis (dotted line), channels cross a zone devoid of rock uplift above a flat HFT segment within the range front. Contacts from field mapping, fold axis from *Mishra and Mukhopadhyay* [2002] and *Thakur et al.*, [2007].

A linear range front and continuous stratigraphic exposure suggest that the 1st-order geologic structure does not vary along strike within a central portion of the Mohand (Figure 2). In this study area, bedrock rivers flow southwest from the divide, traversing down section through Mio-Pleistocene Upper Siwaliks, across a transitional contact, and then across older Middle Siwaliks before reaching the open foreland (Figure 2c) [*Kumar and Nanda*, 1989; *Kumar and Ghosh*, 1991]. The Upper Siwaliks are thick beds of quartzite-cobble conglomerates with a sand matrix and the Middle Siwaliks are poorly indurated multistory sandstones (Figure 3a, c) [*Kumar*, 1993]. The channels have bedrock banks and their beds are covered by sand to cobble-sized sediment with occasional bedrock exposures (Figure 3b, d). Channels occupy most, if not all, of the valley floor and possess steep cut banks and gentler slopes on the inside of meanders bends. Bedload size is limited by the cobble-sized clasts sourced from the Upper Siwaliks conglomerates, the only exception being scattered mass wasting deposits from the Middle Siwaliks hillslopes. Sediment is predominantly transported down the channels during the monsoons (80-85% of the mean annual precipitation, ~1-2 m/yr, occurs July to September [*Bookhagen and Burbank*, 2006; *Mohindra et al.*, 1992] and appears to breakdown to a bi-modal size distribution (sand and cobbles) throughout the channels very quickly (Figure 3). As a result, the channels (a) contain ephemeral rivers characterized by high discharges implying efficient but episodic sediment transport and incision [*Barnes et al.*, 2011] and (b) have an average hydraulic roughness that varies little except where isolated patches of bedrock are exposed.

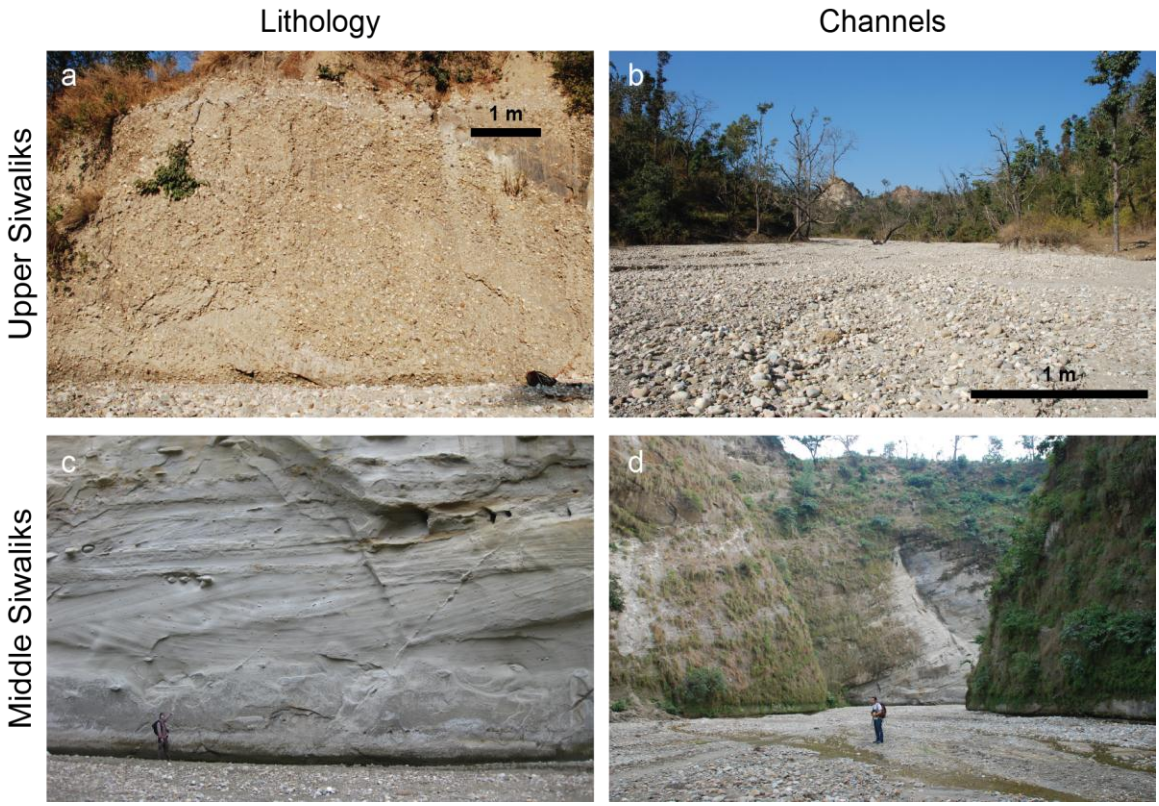

Figure 3. Field photos of the Siwaliks stratigraphy and channel-to-hillslope scale geomorphology in the Mohand range. Upper Siwaliks conglomerates contain cobble-sized clasts within a poorly lithified sandstone matrix (a), and channels that are wide with low banks and hillslope relief (b). Middle Siwaliks contain multistory cross-bedded sandstones (c, with person for scale), and channels that are narrow with steep banks and high hillslope relief (d, with person for scale).

4. METHODS

4.1 Field Data

We investigated the Mohand geology and measured proxies for rock erodibility and channel morphology in selected areas. We augmented existing stratigraphic sections in the Mohand [*Kumar*, 1993; *Kumar and Nanda*, 1989] with our own field observations of the nature and location of the transition from Upper-to-Middle Siwaliks along 5 channels in the area (channels 1, 3, 4, 8, 9 in Figure 2c). We then interpolated between

these locations using the intersection between topography and surfaces projected parallel to average rock orientation.

Rock erodibility exerts a 1st-order control on river incision and channel morphology [*Montgomery and Gran*, 2001; *Whipple*, 2004; *Whipple et al.*, 2000]. Rock strength and fracture spacing is thought to govern bedrock erodibility [e.g. *Hack*, 1957; *Selby*, 1993; *Stock and Montgomery*, 1999]. We quantified intact rock strength using a type N Schmidt Hammer, a spring-loaded device that measures rebound values that scale with unconfined rock strength estimates made in laboratory tests [*Cargill and Shakoor*, 1990; *Selby*, 1993]. We estimated intact rock strength at 10 sites in the Upper Siwaliks and 13 in the Middle Siwaliks by recording 40 rebound measurements per site and discarding all measurements below a rebound value of 11 [*Duvall et al.*, 2004; *Snyder et al.*, 2003a]. In the Upper Siwaliks, we restricted our measurements to the conglomerate matrix because it is the weakest component and thus sets the bedrock strength limit. We also estimated intact rock strength with 'simple means' field testing [*Hack and Huisman*, 2002] because the type N Schmidt Hammer is not designed for weak rocks [*Goudie*, 2006]. This is a semi-quantitative test that classifies a rock's response to hand compression and hammer blows. We conducted 20 simple means testing measurements at each of the same sites. We then compared the mean values of each location and finally combined them into a single average and standard deviation for the two Siwaliks units.

Bedrock erodibility is also affected by fractures because they increase the efficiency of hydraulic plucking and promote bedrock weathering by increasing surface area exposure [*Clarke and Burbank*, 2011; *Hancock et al.*, 2011]. We measured fracture spacing at the same sites where we took intact rock strength measurements. At each site,

we used three 1 m scan lines to quantify fracture spacing perpendicular to bedding, parallel to strike, and parallel to dip [after *Dühnforth et al.*, 2010; *Gillespie et al.*, 1993].

We measured channel form along selected reaches in the field to validate our remote sensing-based estimates because our method is novel and needed testing. We measured bankfull width at 40 locations using a handheld laser range finder and compared these field-based widths to the nearest channel width estimated from the satellite image. We also measured channel slope with a differential GPS along several reaches.

4.2 Remote Sensing

We quantified channel form by combining data extracted from a satellite image and a DEM. We calculated channel width every ~5-7 m from a SPOT-5 satellite image (5 m resolution, *Bouillon et al.* [2006]) with the RivWidth software tool (Figure 4a) [*Pavelsky and Smith*, 2008]. We masked channels from their surroundings by the high contrast between the bright bedload gravels and the adjacent dark vegetation. The mapped channel width corresponds to peak flow, the effective discharge that sets channel form, incises, and transports the largest proportion of bedload downstream in bedrock rivers [*Baker*, 1977; *Lavé and Avouac*, 2001; *Wolman and Miller*, 1960]. We measured channels from ~1 km beyond the mountain front upstream to where they remained visible on the satellite image (blue lines in Figure 2c).

We measured channel elevation and upstream drainage area from the 90 m resolution HydroSHEDS DEM [*Lehner et al.*, 2008] because the 30 m resolution ASTER GDEM V001 and V002 [*Tachikawa et al.*, 2009] produced major errors in the channel pathways and highly stair-stepped profiles. We also report hillslope-scale relief (from

Barnes et al., [2011]) calculated with a modified version of sub-ridgeline relief by *Brocklehurst and Whipple* [2002]. Hillslope relief was measured from the ASTER GDEM V001 because it has a more accurate representation of hillslope gradients than the 90 m DEM [*Barnes et al.*, 2011].

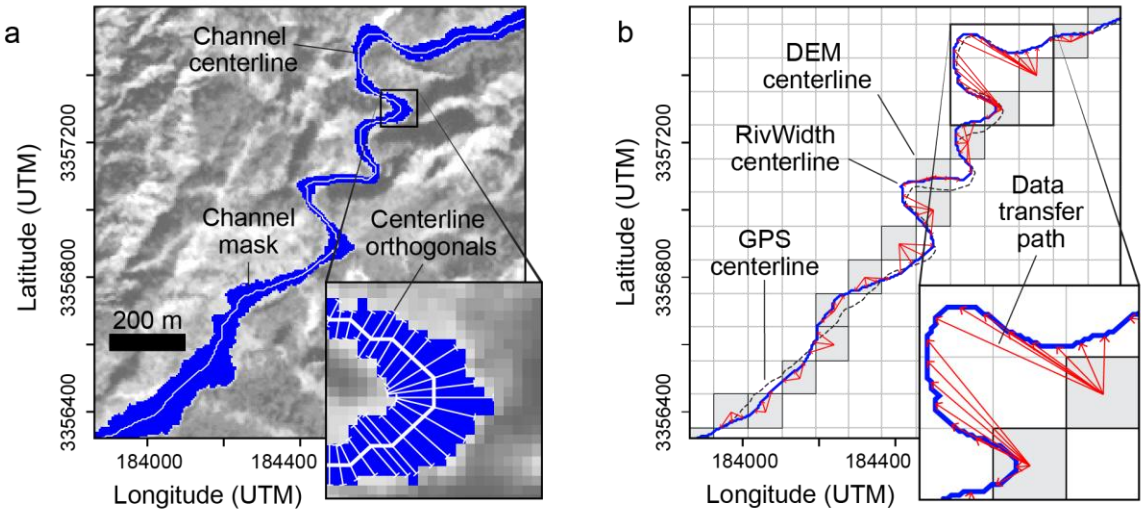

Figure 4. Methods for measuring channel form (location of this example reach in Figure 2c). (a) 5-m resolution SPOT-5 image overlain by RivWidth channel mask (blue) and centerline (white). Inset is channel width (white bars) measured perpendicular to the centerline at each pixel. (b) DEM channel pixels (gray) overlain by channel centerlines determined with RivWidth (blue) and differential-GPS (black) for comparison. Inset shows transfer (red arrows) of DEM-derived information to the image-based channel centerline.

4.3 Data Integration and Calibration of Geomorphic Parameters

We combined the DEM and imaged-based datasets with an algorithm that assigns data from each channel pixel in the DEM to the nearest image-based channel pixel (Figure 4b, Appendix B). Real channel gradients are lower than those estimated from the DEM because the higher resolution image-based channel centerline is longer than the DEM-derived channel centerline. We correct for this inherent overestimation of channel slope by stretching the DEM-based elevations to the image-based channel trace.

To reduce noise associated with the data integration process, we smoothed all parameters downstream using a simple moving average with a window size of 750 m (Figure B1) [after *Duvall et al.*, 2004]. Thus, we avoid interpretations at streamwise length scales <750 m. We calculated sinuosity as the ratio of channel length to straight-line distance between two endpoints spaced 1.5 km along the channel length [e.g. *Mueller*, 1968; *Stark et al.*, 2010]. We empirically determined $\theta_{ref} = 0.5$ in equation (2) from the slope and drainage area data (Figure B2), and calculated steepness (k_{sn}) at every pixel downstream. Similarly, we empirically assigned $b_{ref} = 0.59$ in equation (4) from the width and drainage area data (Figure B3) and calculated wideness (k_{wn}) downstream. To focus on map-view patterns of channel form, we applied a second smoothing of steepness, wideness, and shear stress downstream with a 1 km simple moving average (Figure B1). In map view, we avoid interpretations at streamwise length scales <1.75 km. Finally, when comparing geomorphic parameters between lithologies, we included all channel reaches upstream from the fold axis so that uniform rock uplift rates could be assumed.

We modeled incision potential by combining the Manning formula with the conservation of mass law to obtain the following form of the boundary shear stress formula,

$$\tau_b = \rho g \left(\frac{nQ}{W}\right)^{3/5} S^{7/10}, \quad (5)$$

where ρ is the density of water, g is gravity, and n is the Manning friction factor [e.g. *Snyder et al.*, 2003b; *Yanites et al.*, 2010]. Because measured discharge data is unavailable for the Mohand rivers, we substituted drainage area for discharge,

$$Q = k_q A^c \tag{6}$$

and assumed c = 1, as has been commonly demonstrated [e.g. *Hack*, 1957; *Pazzaglia et al.*, 1998] and assumed [e.g. *Duvall et al.*, 2004; *Montgomery and Gran*, 2001] for regularly-shaped basins with minimal orographic effects. We eliminated the unknown k_q by dividing the boundary shear stress values by the maximum shear stress value, eliminating k_q and creating a shear stress index, τ_{ind} that varies from 0 to 1. This index allows for comparison of relative changes in shear stress rather than absolute values.

5. RESULTS

We analyze changes in lithology, channel geometry, and hillslope relief across the central Mohand range to account for factors influencing channel form. First, we present the stratigraphy and associated erodibility of the Upper and Middle Siwaliks. Second, we validate our remote sensing–based approach and data by comparing the latter with field measurements. We then show large-scale plan-view patterns of channel form to examine the spatial distribution of channel adjustment in relation to tectonics and lithology. Lastly, we examine how variations in channel form and hillslope relief covary downstream.

5.1 Siwalik Stratigraphy and Erodibility

The Upper-to-Middle Siwaliks boundary is ~0.5 km thick, which translates to a ~1 km wide zone in map view (Figures 2 and 5). This zone contains laterally continuous meter to decameter thick conglomerate and sandstone interbeds, with the abundance of conglomerate beds decreasing relative to sandstone beds with increasing distance down section and downstream. Schmidt Hammer measurements show that the mean intact rock strength is 47±29% greater in the Middle Siwaliks compared to the Upper Siwaliks (Figure 5). Testing by simple means shows a similar contrast, with mean intact rock strength of 16.7±8.4 MPa for the Middle Siwaliks compared to 2.9±3.0 MPa for the Upper Siwaliks. Within the transitional contact and also the upper portion of the Middle Siwaliks, intact rock strength gradually increases as the proportion of harder sandstone beds increases relative to weaker conglomerate beds. Fracture spacing is not significantly different between the two rock groups (2.9±1.9 fractures/m for the Middle Siwaliks, 1.8±1.3 for the Upper Siwaliks). We note an ~1 km wide HFT fault zone near the mountain front where the degree of fracturing increases. These results are consistent with previous studies that describe both formations as poorly lithified, but the Middle Siwaliks as comparatively stronger [*Kumar and Tandon*, 1985; *Kumar and Nanda*, 1989].

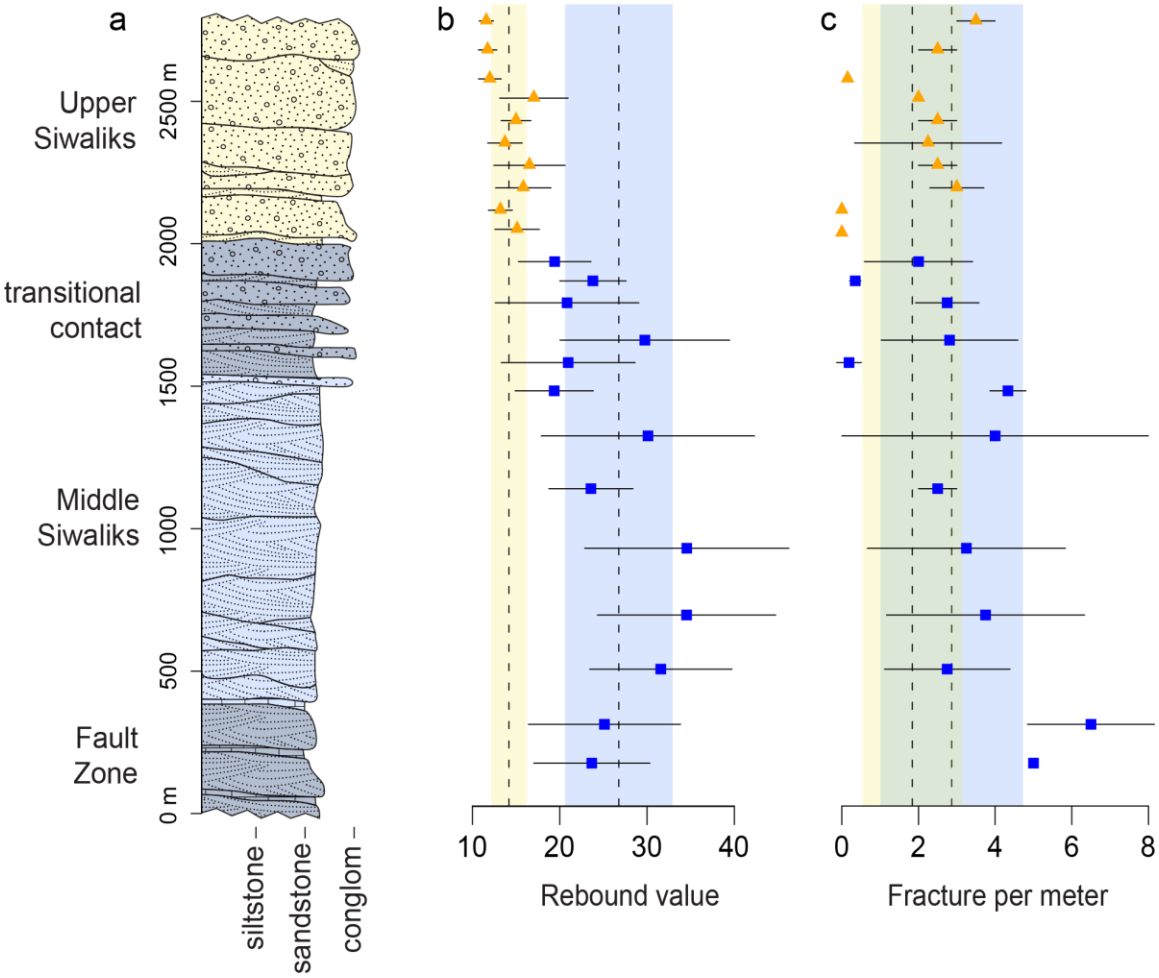

Figure 5. Siwaliks stratigraphy, intact rock strength, and fracture spacing in the Mohand range. Values are means with 1σ errors. (a) Central Mohand stratigraphic column [modified from *Kumar*, 1993; *Kumar and Nanda*, 1989]. Note the transitional contact with increasing sandstone abundance down section. (b) Schmidt Hammer rebound values showing a lower mean (vertical dashed lines) intact rock strength value in the Upper Siwaliks compared to the Middle Siwaliks. This indicates the Middle Siwaliks are less erodible. (c) Fracture spacing measurements indicating no difference in mean (vertical dashed lines) spacing between the Upper and Middle Siwaliks within error. Note the increased degree of fracturing near the mountain front associated with the HFT fault zone.

5.2 Remote Sensing Validation

Stretching the DEM-derived elevation data to the channel trace measured from the satellite image reduces channel slopes (Figure 6a). This process results in more realistic long profiles when compared to GPS measurements made in the field. The

channel gradient reduction occurs in all measured channels and is proportional to the difference in channel length measured from both data sources (Figure 6b). For example, highly sinuous channels that contain tight meander bends (e.g. channel 4) produce greater gradient corrections (Figures 2c and 6c). These corrections influence steepness index, concavity index, and shear stress and thus should be considered when using any low resolution DEM to measure channels with tight meander bends.

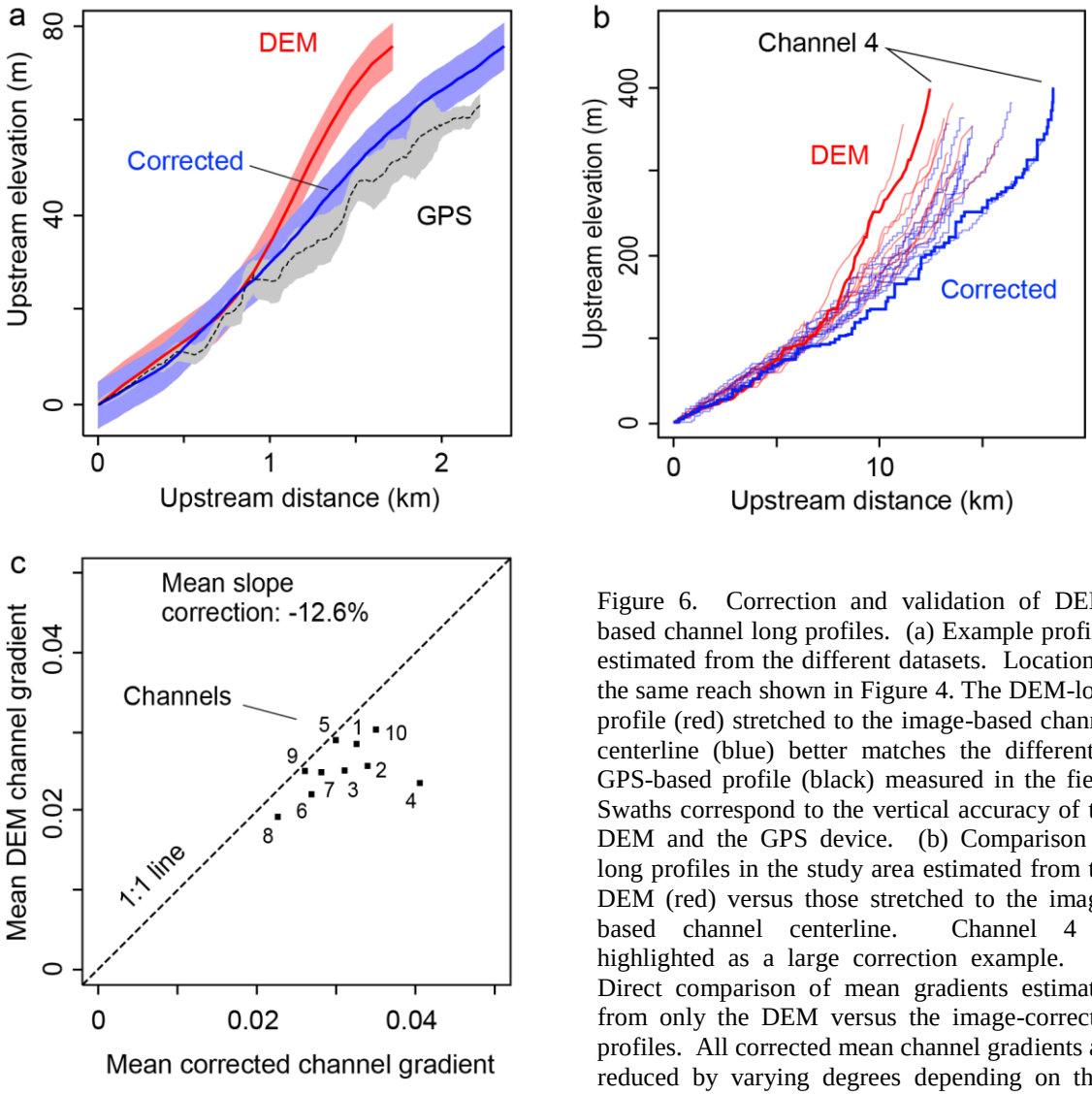

Figure 6. Correction and validation of DEM-based channel long profiles. (a) Example profiles estimated from the different datasets. Location is the same reach shown in Figure 4. The DEM-long profile (red) stretched to the image-based channel centerline (blue) better matches the differential GPS-based profile (black) measured in the field. Swaths correspond to the vertical accuracy of the DEM and the GPS device. (b) Comparison of long profiles in the study area estimated from the DEM (red) versus those stretched to the image-based channel centerline. Channel 4 is highlighted as a large correction example. (c) Direct comparison of mean gradients estimated from only the DEM versus the image-corrected profiles. All corrected mean channel gradients are reduced by varying degrees depending on their sinuosity.

Comparison of channel widths measured in the field and from a satellite image produces a strong 1:1 correlation (Figure 7). On average, there is a small bias for the remotely-sensed data to underestimate true channel width by ~8% (statistically significant at 95% confidence interval, p-value = 0.051). Potential sources of deviations from a 1:1 ratio include channel-masking errors caused by vegetation or hillsides obscuring the channel bed and registration errors between the two datasets such that differently located channel width measurements are compared. Regardless, the robust correlation between the two datasets validates our remote-sensing approach to measuring channel width continuously downstream.

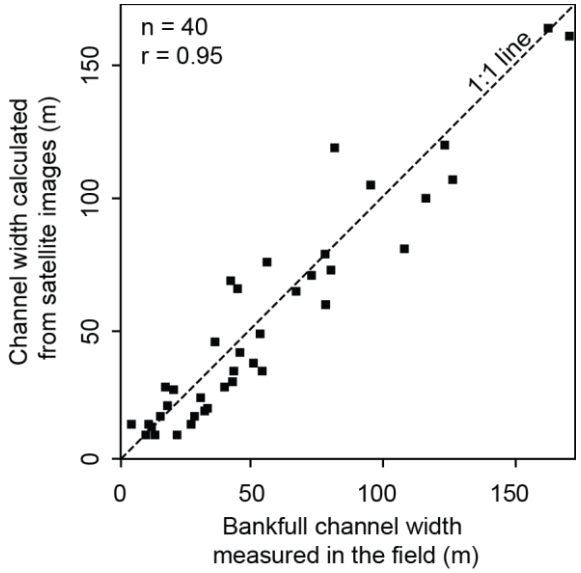

Figure 7. Comparison between image and field-based measurements of channel width. The strong correlation shows the image-based approach accurately measure true channel width in the study area.

5.3 Channel Form vs. Rock Erodibility

Channel reaches in the weak Upper Siwaliks display a relatively wide range of mean slopes yet possess a low range in mean channel widths (Figure 8a), while the inverse is true for the strong Middle Siwaliks. This is in part a function of where each rock type is located along the channel profiles because slope and width do not necessarily vary by the same degree with increasing drainage area (e.g. Figure 1 a, e). Thus, comparing slope and width normalized to drainage area, via steepness (k_{sn}) and wideness (k_{wn}), produces two more comparable parameters (Figure 8b).

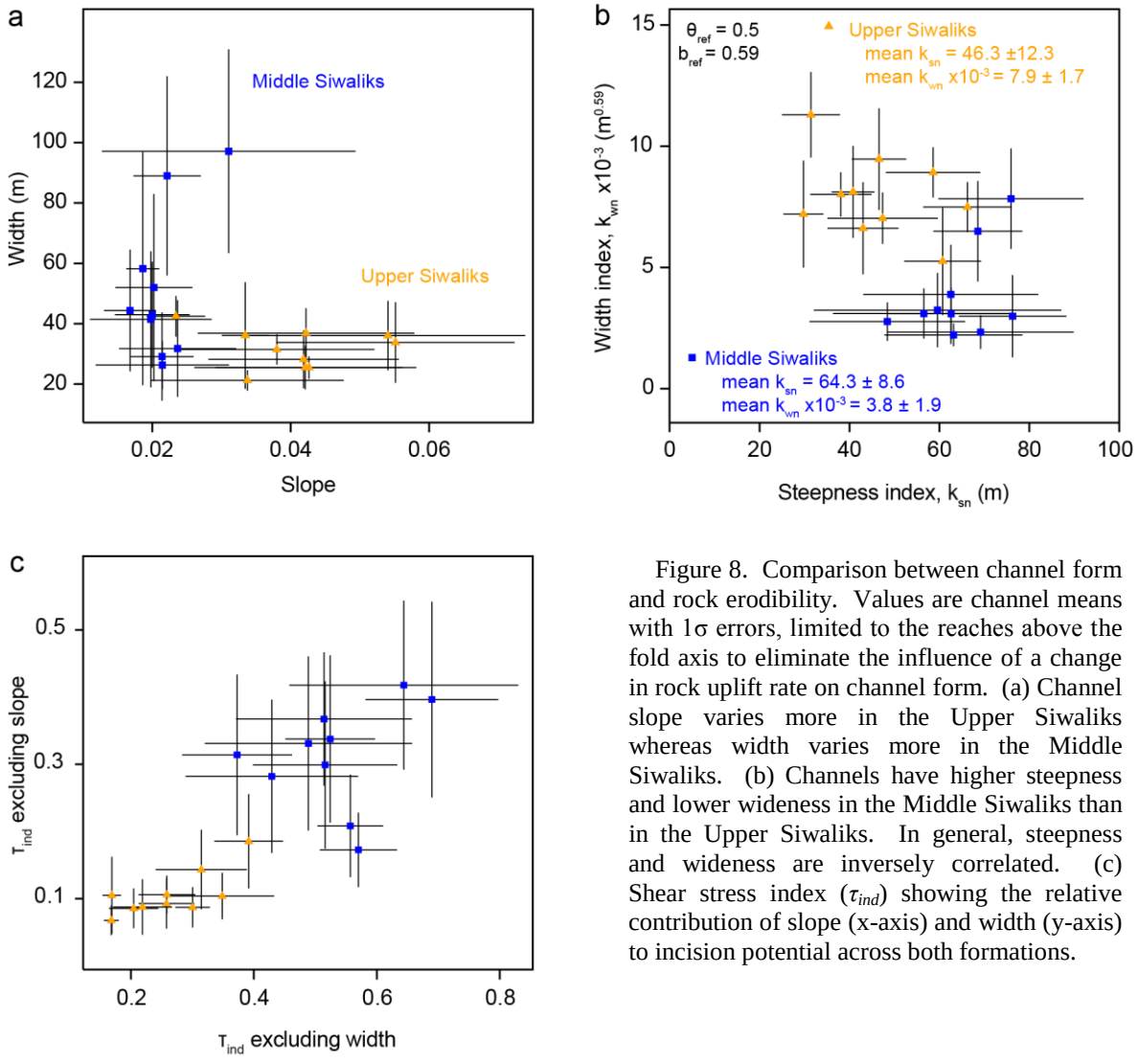

Figure 8. Comparison between channel form and rock erodibility. Values are channel means with 1σ errors, limited to the reaches above the fold axis to eliminate the influence of a change in rock uplift rate on channel form. (a) Channel slope varies more in the Upper Siwaliks whereas width varies more in the Middle Siwaliks. (b) Channels have higher steepness and lower wideness in the Middle Siwaliks than in the Upper Siwaliks. In general, steepness and wideness are inversely correlated. (c) Shear stress index (τ_{ind}) showing the relative contribution of slope (x-axis) and width (y-axis) to incision potential across both formations.

Channels are 32 ± 17% steeper and 70 ± 33% narrower in the Middle Siwaliks than in the Upper Siwaliks. Similarly, using equation 5, shear stress increases in Middle Siwalik channels by 68 ± 13% if only channel slope and upstream drainage area are considered, while shear stress increases by 95 ± 29% when only width and drainage area are considered (Figure 8c). Together, these results indicate that channels both narrow and steepen in response to an increase in substrate strength, thereby focusing erosion potential to erode the stronger uplifting rock.

5.4 Channel Form Patterns

Patterns in channel steepness, wideness, and shear stress are systematic across the study area in plan view. Low steepness in the Upper Siwaliks transitions to an ~2 km-wide zone of high steepness (a knickzone) within the Middle Siwaliks. The position of this knickzone varies somewhat along strike (Figure 9a). All channels exhibit a narrow zone ~4 km-wide oriented along strike that begins within or near the transitional contact and ends ~1-2 km before the range front (Figure 9b). Because shear stress is a function of channel gradient, width, and upstream drainage area, its variations reflect the combined changes in steepness and wideness (Figure 9c). All channels display an ~3 km-wide zone of high shear stress beginning within or near the transitional contact. Values then decrease to a minimum, often before reaching the range front.

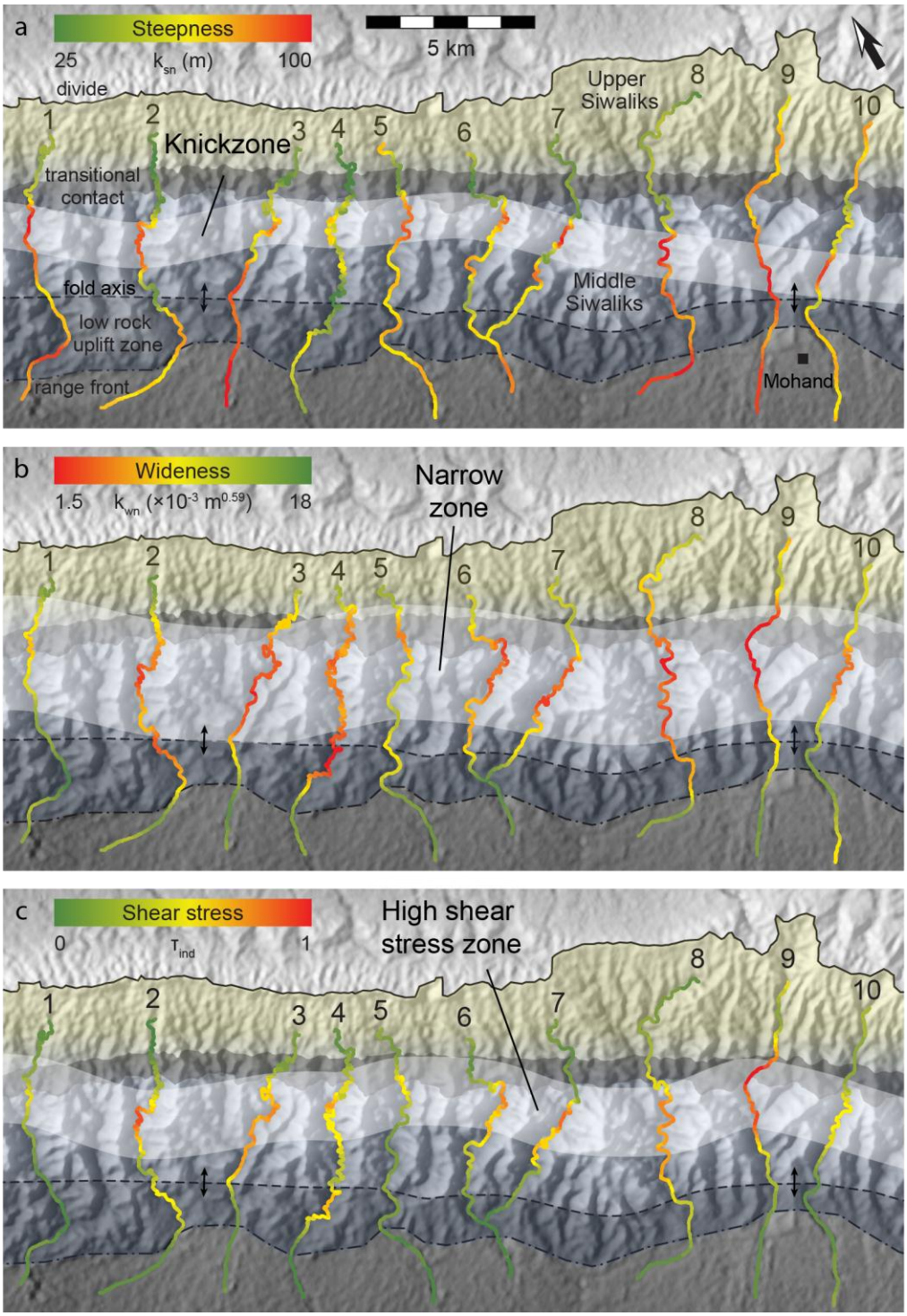

Figure 9. Plan-view patterns of smoothed channel steepness, wideness, and shear stress. (a) Normalized steepness index (k_{sn}) shows a ~2 km-wide knickzone oriented roughly parallel to strike within the Middle Siwaliks. (b) Normalized wideness index (k_{wn}) shows a ~4 km-wide zone of narrow channels across much of the Middle Siwaliks north of the fold axis. Downstream of this zone, channels widen, often before reaching the range front. (c) Shear stress index (τ_{ind}) shows a ~3 km-wide zone of high values, indicative of high relative incision potential within the Middle Siwaliks that reflects the combined effects of channel slope, width, and drainage area.

Variations in channel form also exhibit systematic patterns downstream. First, channels 1-8 reach a local steepness minimum in or just downstream from the transitional contact (dashed red line, Figure 10). This steepness minimum is a knickpoint location and the increase in steepness downstream is a knickzone (e.g. Figure 1c, d). Downstream past this knickzone, steepness patterns either plateau or slightly increase even beyond the range front. Second, wideness decreases downstream beginning within or just upstream from the transitional contact to near the knickpoint (dashed blue line, Figure 10). At the knickpoint, channels reach a threshold wideness of k_{wn} = ~5 x 10^{-3} $m^{0.59}$. Then most channels (except channels 1 and 5) remain narrow until near the range front. Third, in or near the low uplift zone, channels increase their wideness and maintain it into the foreland plain. This width increase is the main reason for the concomitant decrease in shear stress across the low uplift zone and into the foreland. Third, in all channels save 1 and 9, sinuosity peaks within or just downstream from the transitional contact (Figure 11). Where sinuosity peaks, all channels except 1 and 3 show minimal wideness (within ~10% of the minimum).

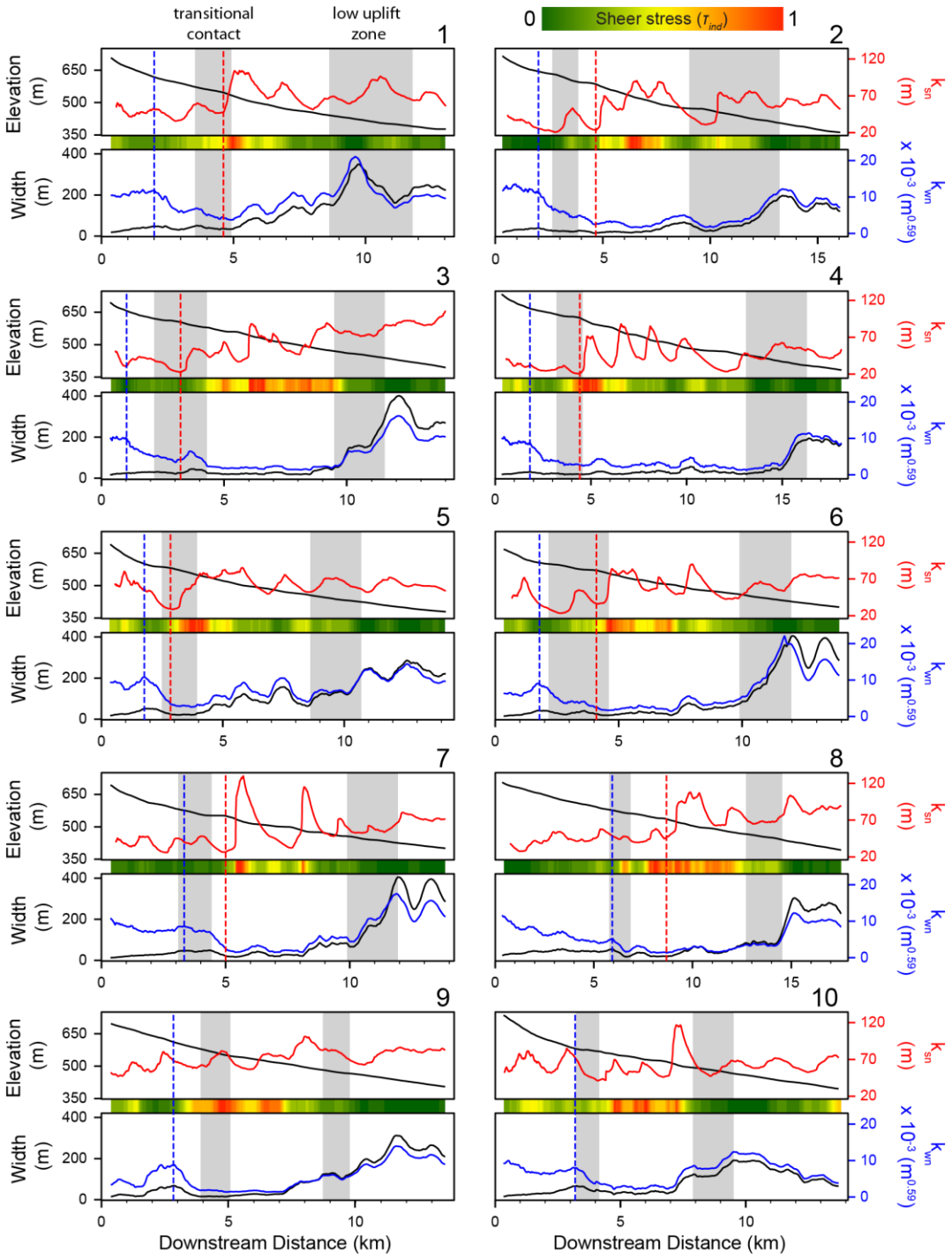

Figure 10. Downstream variations in channel form along all channels. Locations in Figure 2c. Upstream grey bar is the Upper-to-Middle Siwaliks boundary and the downstream bar is the low uplift zone downstream of the fold axis within the range topography (see Figure 2b, c). Upper panel shows elevation profiles (black) and steepness index (k_{sn}, red). Lower panel shows width profiles (black) and wideness index (k_{wn}, blue). Shear stress index (τ_{ind}) is represented by the color gradient between panels. Beginning of channel narrowing (dashed blue line) and knickpoint location (dashed red line) are highlighted. Note all axes have the same values.

Hillslope relief and wideness covary inversely with an average correlation of -0.74±0.25 ($r = -0.82 \pm 0.07$ excluding channel 1). This association holds across both rock formations and alluvial reaches beyond the mountain front (Figure 11). Conversely, hillslope relief and steepness show no correlation ($r = 0 \pm 0.2$) when the entire channel length is considered. However, if only the reaches located upstream from the fold axis are examined, where uplift rates are approximately uniform, high hillslope relief corresponds with steep channels in the Middle Siwaliks (Figure 12a). Similarly, strong lithologies correspond with high hillslope relief and narrow channels (Figure 12b). In summary, wideness is generally low where steepness, sinuosity, hillslope relief, and rock strength are high.

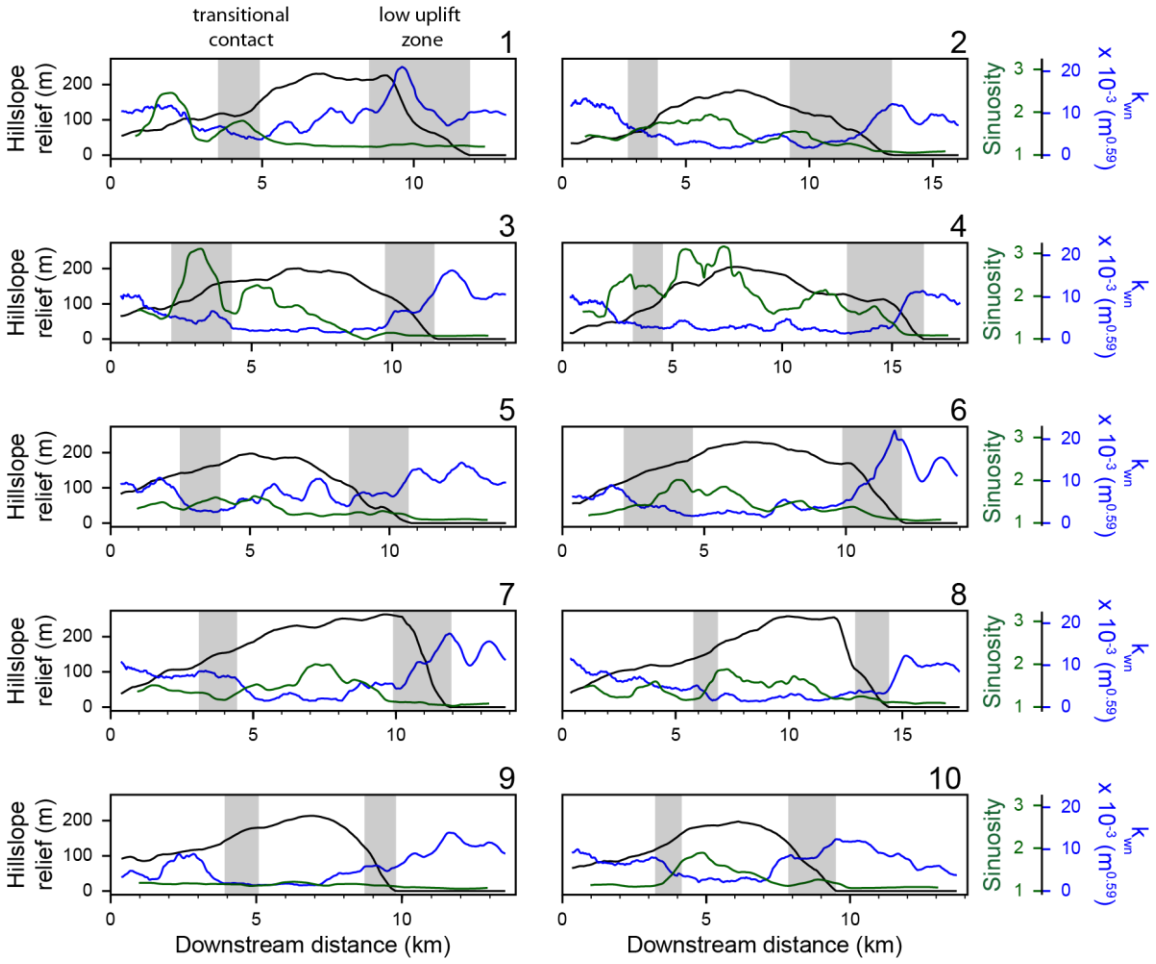

Figure 11. Downstream variations in sinuosity index (green), wideness index (k_{wn}, blue), and hillslope relief (black) along all channels. Upstream grey bar is the Upper-to-Middle Siwaliks boundary and the downstream bar is the low uplift zone downstream of the fold axis within the range topography (see Figure 2b, c). Wideness inversely correlates with hillslope relief and sinuosity.

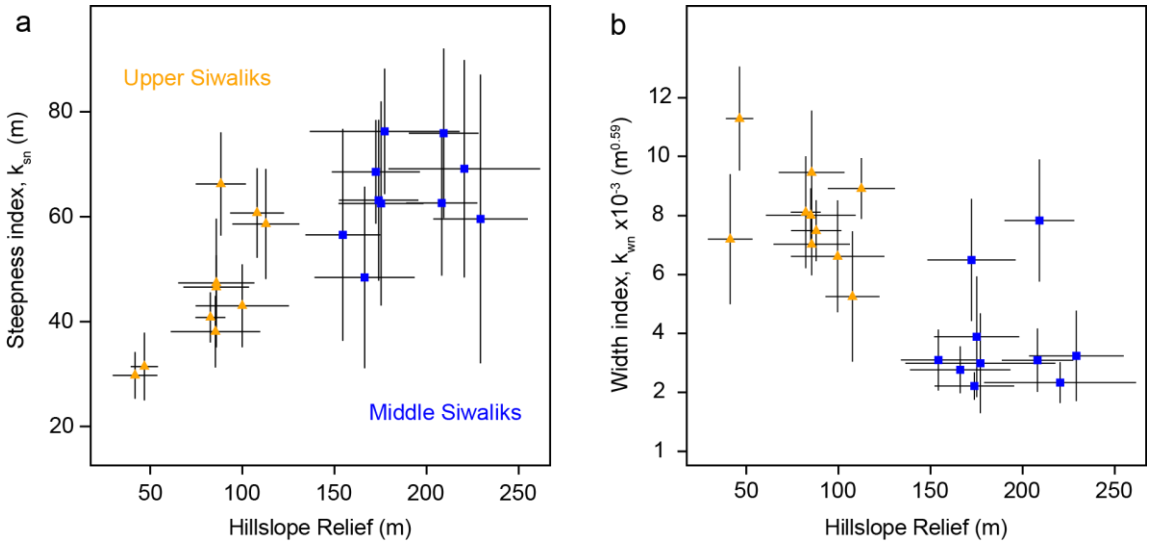

Figure 12. Comparison between hillslope relief, channel form, and rock erodibility. Values are means with 1σ errors, limited to the channel reaches above the fold axis to eliminate the influence of a change in rock uplift rate on channel form. The erosionally-resistant Middle Siwaliks have higher hillslope relief as well as relatively steeper (a) and narrower (b) channels.

6. DISCUSSION

6.1 Channel Steepness and Wideness Controls

By quantifying channel form both vertically and laterally, we gain a more complete understanding of the downstream dynamics and mechanisms of channel adjustment to known changes in rock strength and uplift rate. We observe a knickpoint in most channels within or near the transitional Siwaliks boundary [see also *Kirby and Whipple*, 2012]. Because we infer the rock uplift field to be approximately uniform here, these knickpoints may reflect either a transient wave of enhanced incision rate [e.g. *Harkins et al.*, 2007; *Whittaker et al.*, 2007b], or a change in substrate [e.g. *Haviv et al.*, 2010]. Given the proximity to the change in lithology, we interpret the knickpoints to reflect the change from the weak Upper Siwaliks to the strong Middle Siwaliks. While it is possible that the knickpoints are the result of a recent increase in fault slip rate, the maturity of the fault system, with 4-5 km of displacement, makes this scenario less likely.

Modeling and field studies show that width decreases with increasing slope along knickzones [*Finnegan et al.*, 2005; *Whittaker et al.*, 2007a; *Wobus et al.*, 2006b]. However, in the Mohand, most channels begin narrowing >1 km upstream of the knickpoints and reach a minimal wideness at or near them (Figure 10). To explain this pattern, we hypothesize that as rivers traverse the Siwaliks transition zone where rock strength increases, their channel banks become better able to resist lateral erosion, thus decreasing wideness and enhancing incision potential on the bed. Thus rivers initially maintain a balance between erosivity and rock erodibility by adjusting their shape laterally rather than vertically. Then, as bedrock erodibility continues to decrease downstream, channel wideness reaches a minimum threshold of ~5 x 10^{-3} $m^{0.59}$ (Figure 10), at which point we infer that further narrowing produces less efficient incision due to energy dissipation on the channel banks [*Wobus et al.*, 2008]. At this point, channels cease adjusting their width and instead increase their stream power by steepening, resulting in the formation of a knickzone downstream (Figure 9).

Downstream from the knickzone, most channels remain narrow then dramatically widen in or near the low uplift zone (Figure 10). Here, channels maintain their steepness yet increase their wideness to levels comparable to channels in the alluvial foreland. This wideness increase may reflect (1) an increase in bedrock erodibility induced by brittle deformation of the HFT [e.g. *Kumar et al.*, 2006], (2) backfilling (i.e. aggradation of alluvial sediments) due to increased sedimentation near the range front, and/or (3) a decrease in rock uplift rate. We favor the latter option for several reasons. First, widening begins near the Mohand fold axis, below which the HFT changes from a ~30° ramp to a flat (Figure 2b). This corresponds to a rock uplift rate change from ~7 to

~0 mm/yr. Second, we observed more bedrock exposures in the channel beds near the mountain front, indicating a thin sediment cover, therefore reducing the likelihood of significant backfilling. Third, although rock fracturing is enhanced near the range front and reduces rock strength, the HFT fault zone extends only ~1 km into the range front whereas channel widening begins further upstream.

Shear stress patterns reflect changes in rock strength and uplift rate in steady-state landscapes where incision is balanced by uplift. In response to an increase in rock strength downstream, rivers exert more incision capacity through adjustment of their channel morphologies by widening then steepening. Further downstream, channels respond to a decrease in rock uplift by increasing their width rather than decreasing their slope, an observation made elsewhere in similar settings [e.g. *Lavé and Avouac*, 2001; *Montgomery and Gran*, 2001; *Yanites et al.*, 2010]. This change in channel width but not slope in response to a decrease in rock uplift rate underscores the importance of considering channel width when estimating incision potential patterns and rates in order to infer tectonic information where rock erodibility and uplift are not uniform.

6.2 Channel sinuosity controls

Channels not only steepen and narrow to accommodate greater rock strength of the Middle Siwaliks, they also increase in sinuosity (Figure 11). This is a surprising observation because increased sinuosity lowers average channel slope, lowering the vertical incision potential necessary to balance the increased strength of the Middle Siwaliks. Possible causes for this enhanced meandering include structural control and/or bedload armoring. We explore each of these possibilities here.

Field observations show that rivers flowing against dip tend to exhibit higher sinuosity than those flowing downdip [*Harden,* 1990]. This is because weaker interbeds promote lateral erosion, causing channels to preferentially align parallel to strike, whereas stronger beds tend to resist lateral erosion, directing the channel across strike. While all studied rivers in the Mohand flow across dip, reaches in the upper Middle Siwaliks traverse through sandstone and conglomerate interbeds with highly variable strength (Figure 5). This may explain the peak in sinuosity occurring in most channels within or near the transitional contact (Figure 11). This suggests that small-scale variations in sedimentary layering can significantly impact average channel form and be observed by combining field and remote sensing based measurements.

Another potential mechanism for enhanced sinuosity in the Middle Siwaliks is the role channel sediment plays in controlling vertical and lateral erosion. At low flows, sediment protects the underlying bedrock, but when flow increases to a critical shear stress, sediment is entrained as bedload and acts as tools that enhance bedrock erosion [*Gilbert*, 1877; *Lague et al.*, 2005]. In Mohand, a thick sediment layer almost entirely covers the channel beds whereas the banks are primarily bare bedrock (Figure 3). During lower magnitude/higher frequency flows, only the uppermost bedload is mobilized, thereby eroding the channel banks but not incising into the rock below the bed [*Finnegan et al.*, 2007; *Turowski et al.*, 2008; *Yanites et al.*, 2011]. This process requires an adequate supply of coarse sediment to the channel for a given discharge such that the bed is protected except during high magnitude discharges [*Moore*, 1926; *Snyder et al.*, 2003b]. Such is the case in the Mohand, where the Upper Siwaliks conglomerate provides coarse sediment that promotes lateral erosion.

This process of increased lateral erosion during lower flows can lead to an increase in sinuosity or widening depending on the ratio of river erosivity to bedrock strength. In the strong Middle Siwaliks, the ratio is relatively low, producing banks that resist lateral erosion, confine rivers to narrow channels, and generally influence the plan-view path of the river. During moderate flows, helicoidal currents preferentially erode cut banks causing channels to migrate laterally [*Shepherd*, 1972]. During higher discharge events, sediment is mobilized and vertical incision occurs more evenly across the bed [*Shepherd*, 1972], thereby carving the channel deeper into the sinuous path established by the lower flows. In contrast, we suggest that in the weaker Upper Siwaliks, the ratio of river erosivity to rock erodibility is high resulting in channel banks that are unable to "steer" the river's course. Thus, channels flowing through weak rocks with ample sediment supply tend to widen rather than meander.

6.3 Channel Wideness and Hillslope Relief

Channel wideness and hillslope relief in the Mohand show a strong inverse correlation ($r = -0.74 \pm 0.25$) suggesting that (1) channel width and hillslope relief are shaped by common forces and/or (2) a connection exists between bedrock channel dynamics and hillslope processes. Channel width and hillslope relief share common sources of influence such as lithology, rock uplift rate, and climate [e.g. *Schmidt and Montgomery*, 1995]. Climate does not vary much across the study area, thus rock erodibility and uplift rate are the main factors applicable to both. Given the diverse influences of channel width (e.g. bedload sediment supply and grain size, runoff characteristics, hydraulic roughness, upstream basin characteristics [*Whipple*, 2004]) and

hillslope relief (e.g. valley spacing, soil production, vegetation type and density [*Gabet et al.*, 2004 and references therein]), it is surprising that such a strong correlation exists.

A possible cause for this strong correlation is a connection between bedrock channel dynamics and hillslope processes. The stronger Middle Siwaliks facilitate high hillslope relief and channel banks, producing larger, deeper-seated mass wasting events on the hillslopes near the channel banks. Thus, more debris is delivered to channels in larger magnitude, lower frequency, contributions such that the channels flowing through Middle Siwaliks may be influenced differently than the Upper Siwaliks. At the location of cut bank failures in the Middle Siwaliks, channels are diverted around the foot of the landslide deposit, increasing sinuosity, creating a knickpoint, and narrowing channel width [*Gillespie et al.*, 1993; *Gran and Montgomery*, 2005 2012]. This apparent link of fluvial and hillslope processes may explain the highly scattered relationship between channel width and drainage area in bedrock rivers [e.g. *Montgomery and Gran*, 2001; *Wohl and David*, 2008]. Because hillslope relief can be automatically calculated from DEMs, this relationship could be used to estimate relative variations in channel width directly from a DEM. Further study is needed to determine if hillslope relief and normalized wideness index scale in other settings.

7. SUMMARY AND CONCLUSIONS

Channel form reflects changes in rock strength and uplift rate in the Mohand, if both width and slope are explicitly considered. We hypothesized that channel width may adjust independently of drainage area and/or slope in response to spatial variations in rock strength or uplift rate. We tested this idea on channels draining the Mohand range at

the northwest Himalaya using a new method that integrates continuous measurements of fluvial parameters (channel width, slope, sinuosity, adjacent hillslope relief) from remote sensing data. We observed that channels are 32 ± 17% steeper and 70 ± 33% narrower in the erosionally resistant Middle Siwaliks compared to the weaker Upper Siwaliks. Further, channels begin to narrow to a minimum wideness of ~5 x 10^{-3} $m^{0.59}$ over a kilometer upstream from where they steepen in response to a gradational increase in rock strength associated with a transitional stratigraphic boundary. In response to a decrease in rock uplift rate at the mountain front, channels increase their wideness rather than adjust their steepness. We also observed that rivers flowing across alternating strong and weak beds exhibit increased sinuosity, suggesting that fine-scale variability in bedrock strength via sedimentary interbedding can influence average steepness values. Finally, normalized wideness index scales linearly with hillslope relief in the Mohand range, hinting at a potentially useful proxy for estimating channel width from DEMs. This study highlights the importance of rock strength in influencing channel form and promotes the inclusion of channel width measurements when trying to extract tectonic signals from channel form.

APPENDIX A

WIDENESS INDEX DERIVATION

The wideness index can be used as an empirical measure of deviation from an equilibrium width-area scaling, but it can also be related to incisional potential. The derivation of the wideness index closely follows that of the steepness index [see appendix in *Duvall et al.*, 2004; *Whipple and Tucker*, 1999]. However, rather than assuming channel width scales with drainage area, we rely on the relationship that channel slope exhibits an equilibrium scaling with drainage area as described in equation 1. The wideness index is derived from the stream-power family of models that equate bedrock incision rate (E) to a power function of boundary shear stress (τ_b) which must exceed a threshold of critical shear stress (τ_c),

$$E = k_e\, f(q_s)[\tau_b - \tau_c]^{a_e}, \tag{A1}$$

where k_e depends on rock erodibility, $f(q_s)$ describes the dual role entrained sediment plays as both tools or cover for incision, and a_e depends on the erosion mechanics [*Howard and Kerby*, 1983; *Whipple et al.*, 2000]. We assume that the influence of critical shear stress (τ_c) and entrained sediment ($f(q_s)$) are negligible because (a) the effective discharge that shapes bedrock channels typically far exceeds this value in the Siwalik Hills [*Kirby and Whipple*, 2012], and (b) sediment flux scales with shear stress [*Bagnold*, 1980].

Incision rate is reduced to terms of boundary shear stress, which under steady-uniform flow can be approximated in terms of channel discharge, width, and slope,

$$\tau_b = k_t Q^{\alpha} W^{-\alpha} S^{\beta}, \quad \text{(A2)}$$

where k_t, α, and β are constants that depend on flow resistance dynamics [e.g. *Yanites et al.*, 2010]. Combining (1, 3, 6, A1, and A2) yields,

$$E = K' A^{m'} W^{-n'}, \quad \text{(A3a)}$$

where

$$K' = k_e f(q_s) {k_t}^{a_e} \rho g {k_q}^{\alpha a_e}, \quad \text{(A3b)}$$

$$m' = a_e(\alpha c - \theta\beta), \quad \text{(A3c)}$$

$$n' = b a_e. \quad \text{(A3d)}$$

(A3a) resembles the form of the generalized total stream-power model [*Howard and Kerby*, 1983], except in terms of lateral channel parameters rather than slope.

If steady-state equilibrium conditions exist, such that long term rock uplift rate (U) and bedrock incision rate are balanced and the channel bed elevation does not vary with time ($\frac{dz}{dt} = 0$), then

$$U = E = K' A^{m'} {W_e}^{-n'}, \quad \text{(A4)}$$

which can be rearranged to solve for equilibrium channel width,

$$W_e = (K'/U)^{-n'} A^{m'/n'}. \quad \text{(A5)}$$

This takes the form similar to the width-area formula of (3),

$$W = k_w\, A^b, \quad \text{(A6a)}$$

where k_w is the wideness index, and b is the width exponent with the implied relations,

$$k_w = (K'/U)^{-n'} = (K'/U)^{-ba_e} \quad \text{(9b)}$$

$$b = n'/m' = b/(\alpha c - \theta\beta). \quad \text{(9c)}$$

The width exponent can be empirically determined by plotting channel width and drainage area in log-log space and taking linear regressions of channel reaches that exhibit a steady-exponential widening (Appendix B).

APPENDIX B

DATA INTEGRATION AND SMOOTHING

We developed an algorithm in R code [*Pebesma et al.*, 2012] that integrates, analyzes, and displays channel morphometric data. The algorithm combines topographic information (elevation, upstream drainage area, and hillslope relief) with plan-view channel information (channel width, length, and sinuosity) by assigning data from the nearest DEM pixel to each pixel along the image-based channel centerline (Figure 4b). To reduce error, the algorithm matches data only within the same channel and at, or downstream of, the previous DEM pixel sampled. Because of spatial variability among datasets, DEM pixels are sampled unevenly in the integration processes resulting in a stair stepped pattern on the elevation profiles in the image-corrected dataset (Figure 6b). This stair-step effect, combined with occasional misalignment of tributary junctions between the DEM and image, requires some smoothing of all morphometric variables to reduce noise.

We initially smoothed channel elevation, width, upstream drainage area and hillslope relief data using a downstream simple moving average with a window size of 750 m (Figure B1a, b, d, e, f) [after *Duvall et al.*, 2004]. We then determined the reference concavity index and width exponent by taking the average slope of linear regressions fit to all equilibrium channel reaches (Figure B2, B3) and calculated steepness and wideness indices at every pixel using $\theta_{ref} = 0.5$ and $b_{ref} = 0.59$. Figure 9 shows smoothed normalized steepness, wideness, and shear stress indices using a simple moving average with a window size of 1 km downstream distance, a length necessary to focus on only the large-scale variations in channel shape (Figure B1c, g, h).

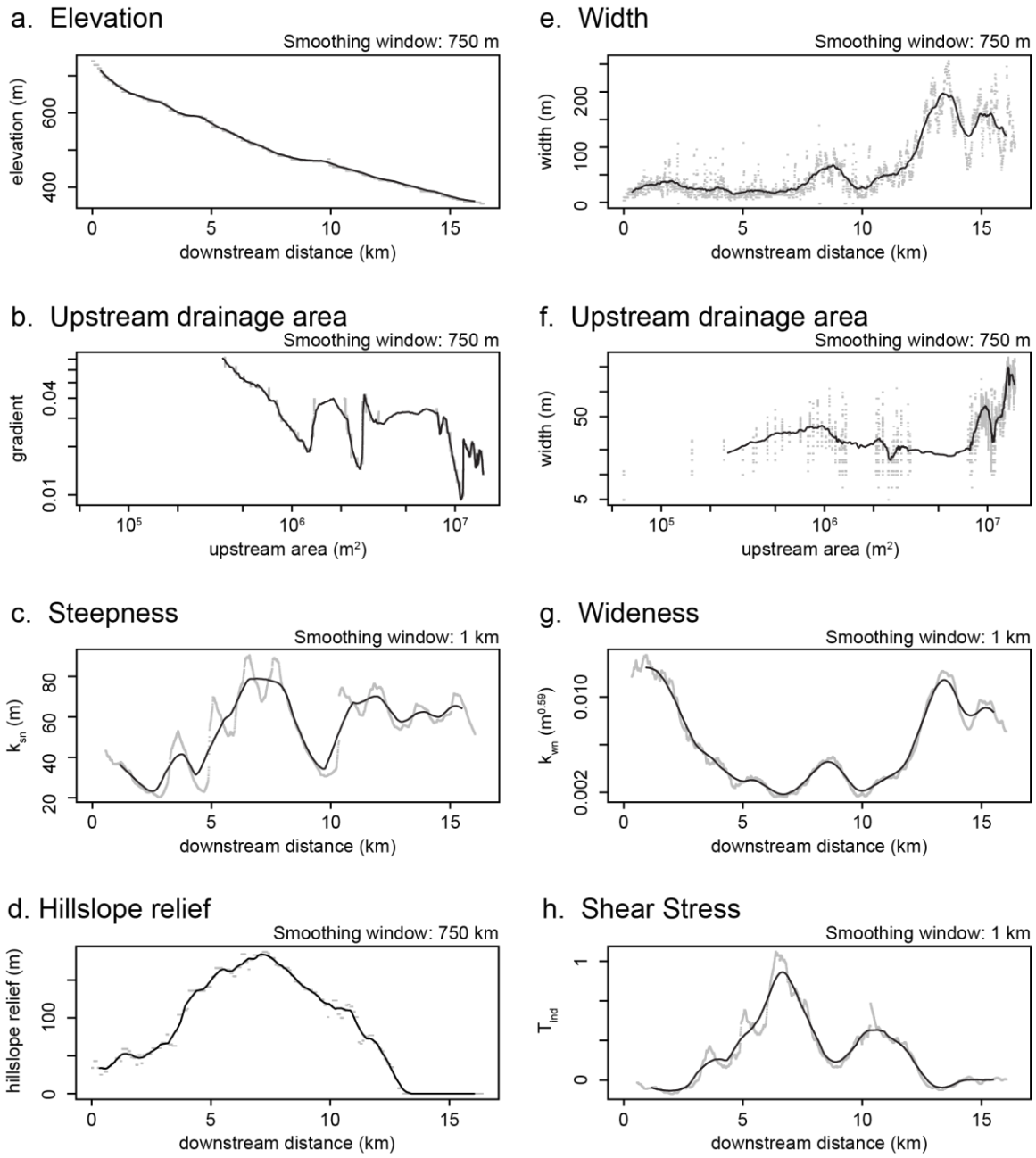

Figure 13. Example channel (2 in Figure 2c) showing raw (gray) and smoothed (black) data. Elevation (a), upstream drainage area (b, f), hillslope relief (d), and width (e), were smoothed with a 750 m simple moving average (Figure 10, 11) [after *Duvall et al.*, 2004]. Steepness (k_{sn}) (c), wideness (k_{wn}), and shear stress (τ_{ind}) (h) indices with a 1 km simple moving average, a window length necessary for the display of large-scale trends in plan view (Figure 9).

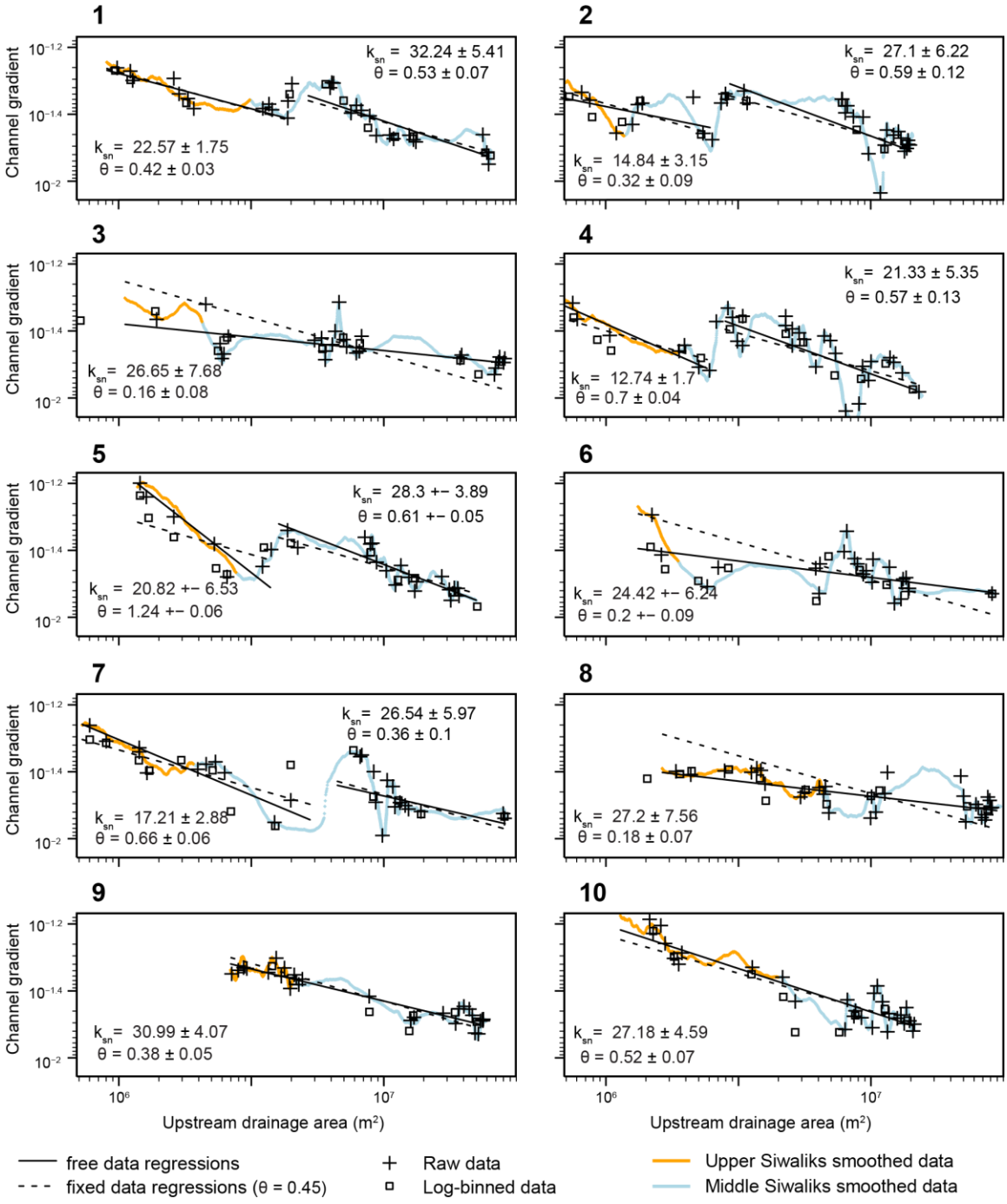

Figure 14. Channel slope versus drainage area for all 10 channels. Lines indicate regression limits applied to equilibrium reaches. Normalized steepness index values are calculated using a reference concavity of 0.45. Average concavity index of the Upper Siwaliks is 0.48, of the Middle Siwaliks is 0.41, and of all equilibrium channel reaches is 0.5.

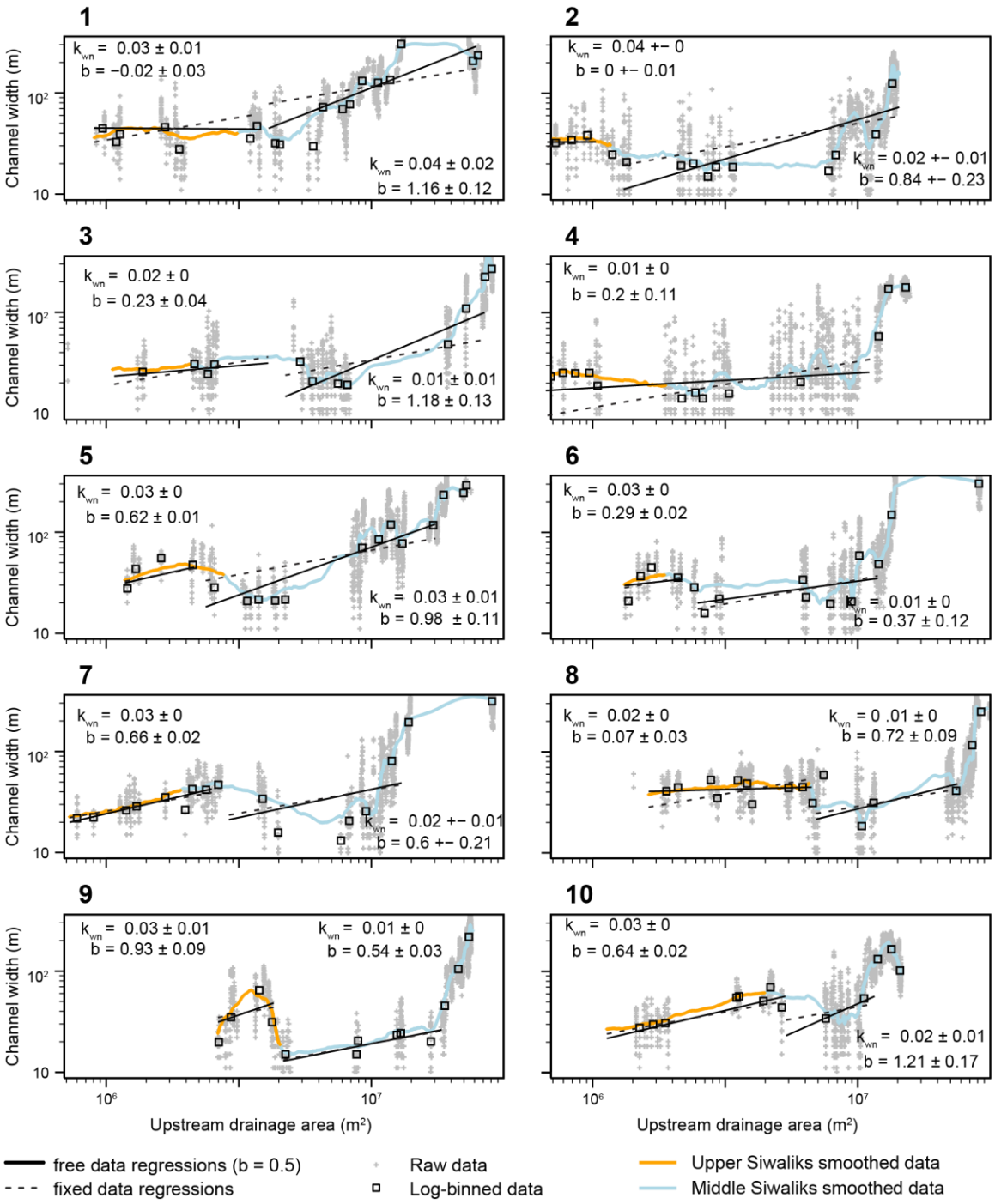

Figure 15. Channel width versus drainage area for all 10 channels. Most channels narrow downstream beyond the transitional contact then widen rapidly before the range front. Lines show regression limits applied to undisturbed reaches. Normalized wideness index values are calculated using a reference width exponent of 0.5. Mean width exponent of the Upper Siwaliks is 0.36, of the Middle Siwaliks is 0.72, and of all equilibrium channel reaches is 0.59.

REFERENCES

Amos, C. B., and D. W. Burbank (2007), Channel width response to differential uplift, *J. Geophys. Res.*, *112*(F2), F02010, doi: 10.1029/2006jf000672.

Anderson, R. S. (1994), Evolution of the Santa Cruz Mountains, California, through tectonic growth and geomorphic decay, *J. Geophys. Res.*, *99*(B10), 20161-20179, doi: 10.1029/94jb00713.

Bagnold, R. A. (1980), An Empirical Correlation of Bedload Transport Rates in Flumes and Natural Rivers, *Proceedings of the Royal Society of London. A. Mathematical and Physical Sciences*, *372*(1751), 453-473, doi: 10.1098/rspa.1980.0122.

Baker, V. R. (1977), Stream-channel response to floods, with examples from central Texas, *Geol. Soc. Am. Bull.*, *88*(8), 1057-1071, doi: 10.1130/0016-7606(1977)88<1057:srtfwe>2.0.co;2.

Barnes, J. B., A. L. Densmore, M. Mukul, R. Sinha, V. Jain, and S. K. Tandon (2011), Interplay between faulting and base level in the development of Himalayan frontal fold topography, *J. Geophys. Res.*, *116*(F3), F03012, doi: 10.1029/2010jf001841.

Bilham, R., K. Larson, and J. Freymueller (1997), GPS measurements of present-day convergence across the Nepal Himalaya, *Nature*, *386*(6620), 61-64, doi: 10.1038/386061a0.

Bookhagen, B., and D. W. Burbank (2006), Topography, relief, and TRMM-derived rainfall variations along the Himalaya, *Geophy. Res. Lett.*, *33*(8), L08405, doi: 10.1029/2006gl026037.

Bouillon, A., M. Bernard, P. Gigord, A. Orsoni, V. Rudowski, and A. Baudoin (2006), SPOT 5 HRS geometric performances: Using block adjustment as a key issue to improve quality of DEM generation, *ISPRS J. Photogram. Rem. Sens.*, *60*(3), 134-146, doi: 10.1016/j.isprsjprs.2006.03.002.

Brocklehurst, S. H., and K. X. Whipple (2002), Glacial erosion and relief production in the Eastern Sierra Nevada, California, *Geomorphology*, *42*(1–2), 1-24, doi: 10.1016/s0169-555x(01)00069-1.

Burbank, D., J. Leland, E. Fielding, R. Anderson, N. Brozovic, M. Reid, and C. Duncan (1996), Bedrock incision, rock uplift and threshold hillslopes in the northwestern Himalayas, *Nature*, *379*(6565), 505-510, doi: 10.1038/379505a0.

Cargill, J. S., and A. Shakoor (1990), Evaluation of empirical methods for measuring the uniaxial compressive strength of rock, *Internat. J.Rock Mechan. Mining Sci. & Geomech. Abstr.*, *27*(6), 495-503, doi: 10.1016/0148-9062(90)91001-n.

Clarke, B. A., and D. W. Burbank (2011), Quantifying bedrock-fracture patterns within the shallow subsurface: Implications for rock mass strength, bedrock landslides, and erodibility, *J. Geophys. Res.*, *116*(F4), F04009, doi: 10.1029/2011jf001987.

Dühnforth, M., R. S. Anderson, D. Ward, and G. M. Stock (2010), Bedrock fracture control of glacial erosion processes and rates, *Geology*, *38*(5), 423-426, doi: 10.1130/g30576.1.

Duvall, A., E. Kirby, and D. Burbank (2004), Tectonic and lithologic controls on bedrock channel profiles and processes in coastal California, *J. Geophys. Res.*, *109*(F3), F03002, doi: 10.1029/2003jf000086.

England, P., and P. Molnar (1997), Active Deformation of Asia: From Kinematics to Dynamics, *Science*, *278*(5338), 647-650, doi: 10.1126/science.278.5338.647.

Finnegan, N. J., L. S. Sklar, and T. K. Fuller (2007), Interplay of sediment supply, river incision, and channel morphology revealed by the transient evolution of an experimental bedrock channel, *J. Geophys. Res.*, *112*(F3), F03S11, doi: 10.1029/2006jf000569.

Finnegan, N. J., G. Roe, D. R. Montgomery, and B. Hallet (2005), Controls on the channel width of rivers: Implications for modeling fluvial incision of bedrock, *Geology*, *33*(3), 229-232, doi: 10.1130/g21171.1.

Flint, J. J. (1974), Stream gradient as a function of order, magnitude, and discharge, *Water Resour. Res.*, *10*(5), 969-973, doi: 10.1029/WR010i005p00969.

Gabet, E. J., B. A. Pratt-Sitaula, and D. W. Burbank (2004), Climatic controls on hillslope angle and relief in the Himalayas, *Geology*, *32*(7), 629-632, doi: 10.1130/g20641.1.

Gilbert, G. K. (1877), Geology of the Henry Mountains (Utah), *U.S. Geog. Geol. Surv. Rocky Mt. reg.*, 160.

Gillespie, P. A., C. B. Howard, J. J. Walsh, and J. Watterson (1993), Measurement and characterisation of spatial distributions of fractures, *Tectonophysics*, *226*(1-4), 113-141, doi: 10.1016/0040-1951(93)90114-Y.

Goode, J. R., and E. Wohl (2010), Substrate controls on the longitudinal profile of bedrock channels: Implications for reach-scale roughness, *J. Geophys. Res.*, *115*(F3), F03018, doi: 10.1029/2008jf001188.

Goudie, A. S. (2006), The Schmidt Hammer in geomorphological research, *Prog. Phys. Geog.*, *30*(6), 703-718, doi: 10.1177/0309133306071954.

Gran, K. B., and D. R. Montgomery (2005), Spatial and temporal patterns in fluvial recovery following volcanic eruptions: Channel response to basin-wide sediment

loading at Mount Pinatubo, Philippines, *Geol. Soc. Am. Bull.*, *117*(1-2), 195-211, doi: 10.1130/b25528.1.

Hack, J. T. (1957), Studies of longitudinal stream profiles in Virginia and Maryland, *US Geol. Surv. Prof. Pap.*, 45-97.

Hack, R., and M. Huisman (2002), Estimating the intact rock strength of a rock mass by simple means, in *9th Congr.of the Int. Ass. Engin. Geol. Env.*, edited by J. L. van Rooy and C. A. Jermy, Engineering Geology for Developing Countries, Durban, South Africa.

Hancock, G. S., E. E. Small, and C. Wobus (2011), Modeling the effects of weathering on bedrock-floored channel geometry, *J. Geophys. Res.*, *116*(F3), F03018, doi: 10.1029/2010jf001908.

Harbor, D. J. (1998), Dynamic Equilibrium between an Active Uplift and the Sevier River, Utah, *J. Geol.*, *106*(2), 181-194, doi: 10.1086/516015.

Harden, D. R. (1990), Controlling factors in the distribution and development of incised meanders in the central Colorado Plateau, *Geol. Soc. Am. Bull.*, *102*(2), 233-242, doi: 10.1130/0016-7606(1990)102<0233:CFITDA>2.3.CO;2.

Harkins, N., E. Kirby, A. Heimsath, R. Robinson, and U. Reiser (2007), Transient fluvial incision in the headwaters of the Yellow River, northeastern Tibet, China, *J. Geophys. Res.*, *112*(F3), F03S04, doi: 10.1029/2006jf000570.

Haviv, I., Y. Enzel, K. X. Whipple, E. Zilberman, A. Matmon, J. Stone, and K. L. Fifield (2010), Evolution of vertical knickpoints (waterfalls) with resistant caprock: Insights from numerical modeling, *J. Geophys. Res.*, *115*(F3), F03028, doi: 10.1029/2008jf001187.

Howard, A. D. (1994), A detachment-limited model of drainage basin evolution, *Water Resour. Res.*, *30*(7), 2261-2285, doi: 10.1029/94wr00757.

Howard, A. D., and G. Kerby (1983), Channel changes in badlands, *Geol. Soc. Am. Bull.*, *94*(6), 739-752, doi: 10.1130/0016-7606(1983)94<739:CCIB>2.0.CO;2.

Kirby, E., and K. Whipple (2001), Quantifying differential rock-uplift rates via stream profile analysis, *Geology*, *29*(5), 415-418, doi: 10.1130/0091-7613(2001)029<0415:qdrurv>2.0.co;2.

Kirby, E., and K. X. Whipple (2012), Expression of active tectonics in erosional landscapes, *J. Struct. Geol.*, doi: 10.1016/j.jsg.2012.07.009.

Kumar, R. (1993), Coalescence megafan: multistorey sandstone complex of the late-orogenic (Mio-Pliocene) sub-Himalayan belt, Dehra Dun, India, *Sed. Geol.*, *85*(1–4), 327-337, doi: 10.1016/0037-0738(93)90091-i.

Kumar, R., and S. K. Tandon (1985), Sedimentology of plio-pleistocene late orogenic deposits associated with intraplate subduction—the Upper Siwalik Subgroup of a part of Panjab Sub-Himalaya, India, *Sed. Geol.*, *42*(1–2), 105-158, doi: 10.1016/0037-0738(85)90076-4.

Kumar, R., and A. C. Nanda (1989), Sedimentology of the Middle Siwalik Subgroup of Mohand area, Dehra Dun Valley, India, *Journal of the Geological Society of India*, *34*(6), 597-616.

Kumar, R., and S. K. Ghosh (1991), Sedimentological Studies of the Upper Siwalik Boulder Conglomerate Formation, Mohand Area, District Saharampur, U.P., *J. Himal. Geol.*, *2*(2), 159-167.

Kumar, S., S. G. Wesnousky, T. K. Rockwell, D. Ragona, V. C. Thakur, and G. G. Seitz (2001), Earthquake Recurrence and Rupture Dynamics of Himalayan Frontal Thrust, India, *Science*, *294*(5550), 2328-2331, doi: 10.1126/science.1066195.

Kumar, S., S. G. Wesnousky, T. K. Rockwell, R. W. Briggs, V. C. Thakur, and R. Jayangondaperumal (2006), Paleoseismic evidence of great surface rupture earthquakes along the Indian Himalaya, *J. Geophys. Res.*, *111*, doi:10.1029/2004JB003309.

Lague, D., N. Hovius, and P. Davy (2005), Discharge, discharge variability, and the bedrock channel profile, *J. Geophys. Res.*, *110*(F4), F04006, doi: 10.1029/2004jf000259.

Langbein, W. B., and L. B. Leopold (1964), Quasi-equilibrium states in channel morphology, *Am. J. Sci.*, *262*(6), 782-794, doi: 10.2475/ajs.262.6.782.

Lavé, J., and J. P. Avouac (2000), Active folding of fluvial terraces across the Siwaliks Hills, Himalayas of central Nepal, *J. Geophys. Res.*, *105*(B3), 5735-5770, doi: 10.1029/1999jb900292.

Lavé, J., and J. P. Avouac (2001), Fluvial incision and tectonic uplift across the Himalayas of central Nepal, *J. Geophys. Res.*, *106*(B11), 26561-26591, doi: 10.1029/2001jb000359.

Lehner, B., K. Verdin, and A. Jarvis (2008), New Global Hydrography Derived From Spaceborne Elevation Data, *Eos Trans. AGU*, *89*(10), doi: 10.1029/2008eo100001.

Leopold, L. B., and T. Maddock, Jr. (1953), The hydraulic geometry of stream channels and physiographic implications, *US Geol. Surv. Prof. Pap.*, 57 pp.

Malik, J. N., and T. Nakata (2003), Active faults and related Late Quaternary deformation along the Northwestern Himalayan Frontal Zone, India, *Annal. Geophys.*, *46*(5), 917-936, doi: 2122/996.

Mishra, P., and D. K. Mukhopadhyay (2002), Balanced structural models of Mohand and Santaurgarh ramp anticlines, Himalayan foreland fold-thrust belt, Dehra Dun re-entrant, Uttaranchal, *Journal of the Geological Society of India*, *60*(6), 649-661.

Mohindra, R., B. Parkash, and J. Prasad (1992), Historical geomorphology and pedology of the Gandak Megafan, Middle Gangetic Plains, India, *Earth Surface Processes and Landforms*, *17*(7), 643-662, doi: 10.1002/esp.3290170702.

Molnar, P., and P. England (1990), Late Cenozoic uplift of mountain ranges and global climate change: chicken or egg?, *Nature*, *346*(6279), 29-34, doi: 10.1038/346029a0.

Montgomery, D. R., and K. B. Gran (2001), Downstream variations in the width of bedrock channels, *Water Resour. Res.*, *37*(6), 1841-1846, doi: 10.1029/2000wr900393.

Montgomery, D. R., and M. T. Brandon (2002), Topographic controls on erosion rates in tectonically active mountain ranges, *Earth Planet. Sci. Lett.*, *201*(3–4), 481-489, doi: 10.1016/s0012-821x(02)00725-2.

Montgomery, D. R., T. B. Abbe, J. M. Buffington, N. P. Peterson, K. M. Schmidt, and J. D. Stock (1996), Distribution of bedrock and alluvial channels in forested mountain drainage basins, *Nature*, *381*(6583), 587-589, doi: 10.1038/381587a0.

Moore, R. C. (1926), Origin of Inclosed Meanders on Streams of the Colorado Plateau, *J. Geol.*, *34*(1), 29-57, doi: 10.1086/623270.

Mueller, J. E. (1968), An Introduction to the Hydraulic and Topographic Sinuosity Indexes, *Annal. Ass. Am. Geog.*, *58*(2), 371-385, doi: 10.1111/j.1467-8306.1968.tb00650.x.

Nakata, T. (1989), Active faults of the Himalaya of India and Nepal, in *Tectonics of the Western Himalayas*, edited by L. L. Malinconico and R. J. Lillie, pp. 243-264, Geol. Soc. Am. Spec. Paps. .

Ouimet, W. B., K. X. Whipple, and D. E. Granger (2009), Beyond threshold hillslopes: Channel adjustment to base-level fall in tectonically active mountain ranges, *Geology*, *37*(7), 579-582, doi: 10.1130/g30013a.1.

Pavelsky, T. M., and L. C. Smith (2008), RivWidth: A Software Tool for the Calculation of River Widths From Remotely Sensed Imagery, *Geosci. Remote Sens. Lett., IEEE*, *5*(1), 70-73, doi: 10.1109/lgrs.2007.908305.

Pazzaglia, F. J., T. W. Gardner, and D. J. Merritts (1998), Bedrock fluvial incision and longitudinal profile development over geologic time scales determined by fluvial terraces, in *Rivers Over Rock: Fluvial Processes in Bedrock Channels*, edited, pp. 207-235, AGU, Washington, DC.

Pebesma, E., D. Nüst, and R. Bivand (2012), The R software environment in reproducible geoscientific research, *Eos Trans. AGU*, *93*(16), doi: 10.1029/2012eo160003.

Powers, P. M., R. J. Lillie, and R. S. Yeats (1998), Structure and shortening of the Kangra and Dehra Dun reentrants, Sub-Himalaya, India, *Geol. Soc. Am. Bull.*, *110*(8), 1010-1027, doi: 10.1130/0016-7606(1998)110<1010:sasotk>2.3.co;2.

Raiverman, V., A. Mukerjea, M. K. Saproo, S. V. Kunte, and J. Ram (1990), Geological map of Himalayan foothills between Yamuna and Sarda rivers, Keshava Deva Malaviya Institute of Petrolium Exploration, Oil and Natural Gas Corporation, Dehra Dun, India.

Rao, Y. S. N., A. A. Rahman, and D. P. Rao (1975), On the structure of the Siwalik Range between the rivers Yamuna and Ganga, *Himalayan Geology*, *4*, 137-150.

Sangode, S. J., and R. Kumar (2003), Magnetostratigraphic correlation of the Late Cenozoic fluvial sequences from NW Himalaya, India, *Current Sci.*, *84*(8).

Schmidt, D., and D. Montgomery (1995), Limits to relief, *Science*, *270*(5236), 617-620, doi: 10.1126/science.270.5236.617.

Selby, M. J. (1993), *Hillslope Materials and Processes*, Second ed., Oxford University Press, Oxford, UK.

Shepherd, R. G. (1972), Incised River Meanders: Evolution in Simulated Bedrock, *Science*, *178*(4059), 409-411, doi: 10.1126/science.178.4059.409.

Sklar, L., and W. E. Dietrich (1998), River longitudinal profiles and bedrock incision models; stream power and the influence of sediment supply, in *Rivers Over Rock: Fluvial Processesin Bedrock Channels*, edited by K. J. Tinkler and E. E. Wohl, pp. 237-260, Geophysical Monograph Series.

Snyder, N. P., K. X. Whipple, G. E. Tucker, and D. J. Merritts (2003a), Channel response to tectonic forcing: field analysis of stream morphology and hydrology in the Mendocino triple junction region, northern California, *Geomorphology*, *53*(1–2), 97-127, doi: 10.1016/s0169-555x(02)00349-5.

Snyder, N. P., K. X. Whipple, G. E. Tucker, and D. J. Merritts (2003b), Importance of a stochastic distribution of floods and erosion thresholds in the bedrock river incision problem, *J. Geophys. Res.*, *108*(B2), 2117, doi: 10.1029/2001jb001655.

Stark, C. P. (2006), A self-regulating model of bedrock river channel geometry, *Geophysical Research Letters*, *33*(4), L04402, doi: 10.1029/2005gl023193.

Stark, C. P., J. R. Barbour, Y. S. Hayakawa, T. Hattanji, N. Hovius, H. Chen, C.-W. Lin, M.-J. Horng, K.-Q. Xu, and Y. Fukahata (2010), The Climatic Signature of Incised River Meanders, *Science*, *327*(5972), 1497-1501, doi: 10.1126/science.1184406.

Stock, J. D., and D. R. Montgomery (1999), Geologic constraints on bedrock river incision using the stream power law, *J. Geophys. Res.*, *104*(B3), 4983-4993, doi: 10.1029/98jb02139.

Stølum, H.-H. (1996), River Meandering as a Self-Organization Process, *Science*, *271*(5256), 1710-1713, doi: 10.1126/science.271.5256.1710.

Tachikawa, T., et al. (2009), Advanced Spaceborne Thermal Emission and Reflection Radiometer (ASTER) Global Digital Elevation Model, edited by METI and NASA, Land Processes Distributed Active Archive Center (LP DAAC).

Thakur, V. C., A. K. Pandey, and N. Suresh (2007), Late Quaternary–Holocene evolution of Dun structure and the Himalayan Frontal Fault zone of the Garhwal Sub-Himalaya, NW India, *J. Asian Earth Sci.*, *29*(2–3), 305-319, doi: 10.1016/j.jseaes.2006.02.002.

Tomkin, J. H., M. T. Brandon, F. J. Pazzaglia, J. R. Barbour, and S. D. Willett (2003), Quantitative testing of bedrock incision models for the Clearwater River, NW Washington State, *J. Geophys. Res.*, *108*(B6), 2308, doi: 10.1029/2001jb000862.

Turowski, J. M., N. Hovius, H. Meng-Long, D. Lague, and C. Men-Chiang (2008), Distribution of erosion across bedrock channels, *Earth Surf. Process. Landforms*, *33*, 353-363, doi: 10.1002/esp.1559.

Walsh, L. S., A. J. Martin, T. P. Ojha, and T. Fedenczuk (2012), Correlations of fluvial knickzones with landslide dams, lithologic contacts, and faults in the southwestern Annapurna Range, central Nepalese Himalaya, *J. Geophys. Res.*, *117*(F1), F01012, doi: 10.1029/2011jf001984.

Wesnousky, S. G., S. Kumar, R. Mohindra, and V. C. Thakur (1999), Uplift and convergence along the Himalayan Frontal Thrust of India, *Tectonics*, *18*(6), 967-976, doi: 10.1029/1999tc900026.

Whipple, K. X. (2004), Bedrock Rivers and the Geomorphology of Active Orogens, *Annual Rev. Earth Planet. Sci.*, *32*(1), 151-185, doi: doi:10.1146/annurev.earth.32.101802.120356.

Whipple, K. X., and G. E. Tucker (1999), Dynamics of the stream-power river incision model: Implications for height limits of mountain ranges, landscape response timescales, and research needs, *J. Geophys. Res.*, *104*(B8), 17661-17674, doi: 10.1029/1999jb900120.

Whipple, K. X., G. S. Hancock, and R. S. Anderson (2000), River incision into bedrock: Mechanics and relative efficacy of plucking, abrasion, and cavitation, *Geol. Soc. Am. Bull.*, *112*(3), 490-503, doi: 10.1130/0016-7606(2000)112<490:riibma>2.0.co;2.

Whittaker, A. C. (2012), How do landscapes record tectonics and climate?, *Lithosphere*, *4*(2), 160-164, doi: 10.1130/rf.l003.1.

Whittaker, A. C., P. A. Cowie, M. Attal, G. E. Tucker, and G. P. Roberts (2007a), Contrasting transient and steady-state rivers crossing active normal faults: new field observations from the Central Apennines, Italy, *Basin Research*, *19*(4), 529-556, doi: 10.1111/j.1365-2117.2007.00337.x.

Whittaker, A. C., P. A. Cowie, M. l. Attal, G. E. Tucker, and G. P. Roberts (2007b), Bedrock channel adjustment to tectonic forcing: Implications for predicting river incision rates, *Geology*, *35*(2), 103-106, doi: 10.1130/g23106a.1.

Whittaker, A. C., M. Attal, P. A. Cowie, G. E. Tucker, and G. Roberts (2008), Decoding temporal and spatial patterns of fault uplift using transient river long profiles, *Geomorphology*, *100*(3–4), 506-526, doi: 10.1016/j.geomorph.2008.01.018.

Wobus, C., K. X. Whipple, E. Kirby, N. Snyder, J. Johnson, K. Spyropolou, B. Crosby, and D. Sheehan (2006a), Tectonics from topography: Procedures, promise, and pitfalls, in *Geological Society of America Special Papers*, edited, pp. 55-74.

Wobus, C. W., G. E. Tucker, and R. S. Anderson (2006b), Self-formed bedrock channels, *Geophys. Res. Lett.*, *33*(18), L18408, doi: 10.1029/2006gl027182.

Wobus, C. W., J. W. Kean, G. E. Tucker, and R. S. Anderson (2008), Modeling the evolution of channel shape: Balancing computational efficiency with hydraulic fidelity, *J. Geophys. Res.*, *113*(F2), F02004, doi: 10.1029/2007jf000914.

Wohl, E. (2004), Limits of downstream hydraulic geometry, *Geology*, *32*(10), 897-900, doi: 10.1130/g20738.1.

Wohl, E., and G. C. L. David (2008), Consistency of scaling relations among bedrock and alluvial channels, *J. Geophys. Res.*, *113*(F4), F04013, doi: 10.1029/2008jf000989.

Wolman, M. G., and J. P. Miller (1960), Magnitude and frequency of forces in geomorphic processes, *J. Geol.*, *68*(1), 54-74, doi: 10.1086/626637.

Yanites, B. J., G. E. Tucker, H.-L. Hsu, C.-c. Chen, Y.-G. Chen, and K. J. Mueller (2011), The influence of sediment cover variability on long-term river incision rates: An example from the Peikang River, central Taiwan, *J. Geophys. Res.*, *116*(F3), F03016, doi: 10.1029/2010jf001933.

Yanites, B. J., G. E. Tucker, K. J. Mueller, Y.-G. Chen, T. Wilcox, S.-Y. Huang, and K.-W. Shi (2010), Incision and channel morphology across active structures along the Peikang River, central Taiwan: Implications for the importance of channel width, *Geol. Soc. Am. Bull.*, *122*(7-8), 1192-1208, doi: 10.1130/b30035.1.

Yeats, R. S., and R. J. Lillie (1991), Contemporary tectonics of the Himalayan frontal fault system: folds, blind thrusts and the 1905 Kangra earthquake, *J. Struct. Geol.*, *13*(2), 215-225, doi: 10.1016/0191-8141(91)90068-t.

Yeats, R. S., and V. C. Thakur (2008), Active faulting south of the Himalayan Front: Establishing a new plate boundary, *Tectonophysics*, *453*(1–4), 63-73, doi: 10.1016/j.tecto.2007.06.017.